

# Multitargeted Immunomodulatory Therapy for Viral Myocarditis by Engineered Extracellular Vesicles

Weiya Pei,<sup>1</sup> Yingying Zhang,<sup>1</sup> Xiaolong Zhu,<sup>1</sup> Chen Zhao, Xueqin Li, Hezuo Lü,<sup>\*</sup> and Kun Lv<sup>\*</sup>



Cite This: <https://doi.org/10.1021/acsnano.3c05847>



Read Online

ACCESS |



Metrics & More



Article Recommendations

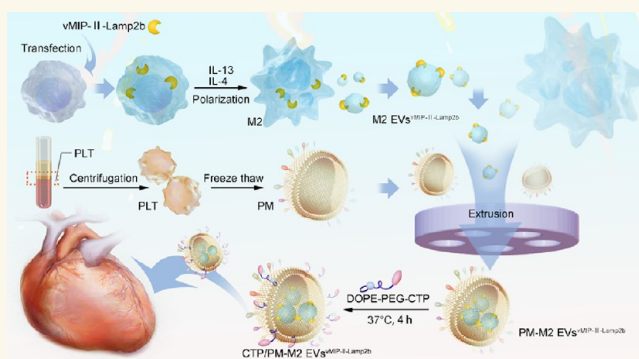


Supporting Information

**ABSTRACT:** Immune regulation therapies are considered promising for treating classically activated macrophage (M1)-driven viral myocarditis (VM). Alternatively, activated macrophage (M2)-derived extracellular vesicles (M2 EVs) have great immunomodulatory potential owing to their ability to reprogram macrophages, but their therapeutic efficacy is hampered by insufficient targeting capacity in vivo. Therefore, we developed cardiac-targeting peptide (CTP) and platelet membrane (PM)-engineered M2 EVs enriched with viral macrophage inflammatory protein-II (vMIP-II), termed CTP/PM-M2 EVs<sup>vMIP-II-Lamp2b</sup>, to improve the delivery of EVs “cargo” to the heart tissues. In a mouse model of VM, the intravenously injected CTP/PM-M2 EVs<sup>vMIP-II-Lamp2b</sup> could be carried into the

myocardium via CTP, PM, and vMIP-II. In the inflammatory microenvironment, macrophages differentiated from circulating monocytes and macrophages residing in the heart showed enhanced endocytosis rates for CTP/PM-M2 EVs<sup>vMIP-II-Lamp2b</sup>. Subsequently, CTP/PM-M2 EVs<sup>vMIP-II-Lamp2b</sup> successfully released functional M2 EVs<sup>vMIP-II-Lamp2b</sup> into the cytosol, which facilitated the reprogramming of inflammatory M1 macrophages to reparative M2 macrophages. vMIP-II not only helps to increase the targeting ability of M2 EVs but also collaborates with M2 EVs to regulate M1 macrophages in the inflammatory microenvironment and downregulate the levels of multiple chemokine receptors. Finally, the cardiac immune microenvironment was protectively regulated to achieve cardiac repair. Taken together, our findings suggest that CTP-and-PM-engineered M2 EVs<sup>vMIP-II-Lamp2b</sup> represent an effective means for treating VM and show promise for clinical applications.

**KEYWORDS:** Macrophages, Platelet membranes, Extracellular vesicles, Viral myocarditis, Immunomodulation



## INTRODUCTION

Viral myocarditis (VM) has an incidence rate of 10–22 per 100 000 individuals.<sup>1</sup> Most patients present with subclinical or insidious symptoms, while a few develop fulminant myocarditis, which is associated with impairment of cardiac function and hemodynamic disorders. Moreover, some patients with recurrent symptoms can develop chronic myocarditis and dilated cardiomyopathy, leading to the eventual need for heart transplantation.<sup>2</sup> Viral infections, especially those of enterovirus coxsackievirus B3 (CVB3), an unenveloped, single-stranded, positive-stranded small RNA virus involved in myocardium-induced VM, are one of the main contributors to sudden unexplained death in adolescents.<sup>3</sup>

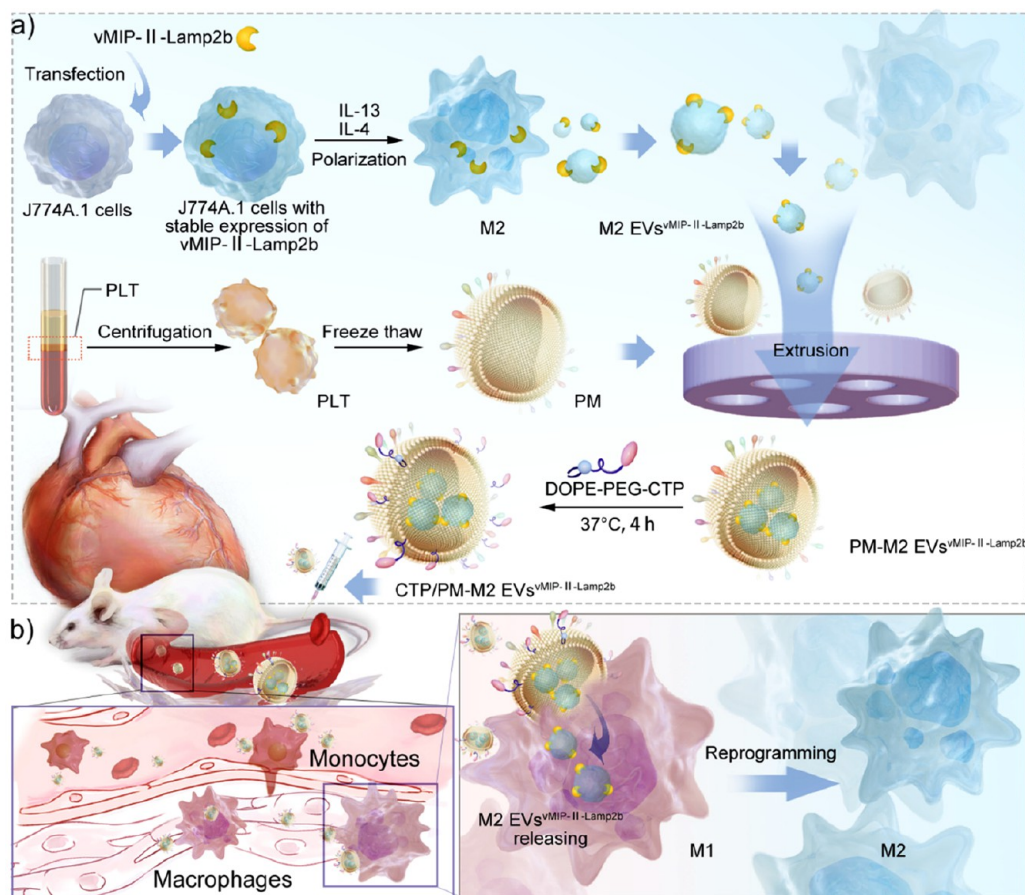
In addition to CVB3 damage to the heart, there is growing evidence to suggest that cardiomyocyte damage induced by host immune responses plays a key role in the pathogenesis of VM.<sup>4</sup> As a key effector cell of the immune system, macrophages are essential for cardiac homeostasis and

myocardial repair and represent one of the earliest and most dominant subpopulations of cardiac infiltrating cells in the early stage of VM.<sup>5,6</sup> Among them, M1 macrophages are the key cells driving VM.<sup>7–9</sup> Indeed, increasing evidence suggests that prolonged and excessive presence of M1 macrophages aggravates the inflammatory reaction and disrupts the repair phase, indicating that the regulation of macrophage polarization is essential for myocardial repair.<sup>7</sup> Therefore, the development of an effective treatment for M1 macrophage regulation is of great practical significance for improving the

**Received:** June 28, 2023

**Revised:** January 3, 2024

**Accepted:** January 8, 2024

Scheme 1. Schematic Illustration of the Fabrication of CTP/PM-M2 EVs<sup>vMIP-II-Lamp2b</sup>

<sup>a</sup>CTP/PM-M2 EVs<sup>vMIP-II-Lamp2b</sup> effectively bound M1 macrophages and reprogrammed them to M2 macrophages in the hearts of mice with viral myocarditis for immunomodulatory effects.

quality of life of patients and reducing the social medical burden.

Extracellular vesicles (EVs) are membrane nanovesicles containing a variety of bioactive molecules, including RNA, DNA, and proteins,<sup>10</sup> which play an important role in immunoregulation and tissue regeneration and are rapidly gaining attention as an emerging treatment method in various disease fields.<sup>11–13</sup> Previous studies have shown that mice with adoptive metastasis of M2 macrophages showed less cardiac inflammation, indicating the protective role of M2 macrophages in VM.<sup>14–16</sup> However, whether M2 EVs mediate protective effects in the VM remains unknown. Although EVs have obvious advantages over traditional nanostructures, such as low immunogenicity and tissue permeability independent of the EPR (enhanced permeability and retention) effect, their therapeutic effect is still greatly reduced due to their short half-life and poor targeting ability to specific cell types and tissues.<sup>17–19</sup>

Multiple studies have shown significantly increased levels of macrophage-associated chemokine receptor expression in VM, leading to myocardial damage and immune cell infiltration.<sup>20–22</sup> Therefore, we believe that M2 EVs can be modified with a chemokine receptor antagonist as one target to gather and target the injured site. Viral macrophage inflammatory protein-II (vMIP-II) is a broad-spectrum chemokine receptor antagonist peptide, which can cooperate with M2 EVs to regulate M1 macrophages in the inflammatory microenviron-

ment, downregulate the levels of multiple chemokine receptors, and competitively inhibit multiple chemokine signaling pathways.<sup>23,24</sup> Lysosome-associated membrane protein 2b (Lamp2b) is an EV-specific membrane protein and is an important component in the formation of EVs. Therefore, we used DNA recombination technology to fuse the vMIP-II DNA sequence to Lamp2b enriched on the EVs' surface to form a fusion protein (vMIP-II-Lamp2b). Finally, vMIP-II and Lamp2b were coexpressed in M2 EVs, termed M2 EVs<sup>vMIP-II-Lamp2b</sup>.

Recently, platelet membranes (PM) have been introduced onto the surfaces of exosomes and nanoparticles to construct biomimetic nanoplateforms that mimic the cellular homing ability of platelets to target multiple diseases.<sup>25,26</sup> As platelets adhere to the damaged endothelium via several specialized proteins expressed on their cell membranes and have an intrinsic affinity to the site of inflammation,<sup>27</sup> modifying engineered M2 EVs<sup>vMIP-II-Lamp2b</sup> with a second target-PM can enhance the targeted delivery of EVs to damaged myocardium. Meanwhile, the third target, cardiac-targeting peptide (CTP, APWHLSSQYSRT), will load on the surface of M2 EVs<sup>vMIP-II-Lamp2b</sup> to form CTP/PM-M2 EVs<sup>vMIP-II-Lamp2b</sup> (Scheme 1). Our research is based on the hypothesis that CTP-andPM-engineered M2 EVs<sup>vMIP-II-Lamp2b</sup> can be delivered to the heart and exert therapeutic effects on CVB3-induced VM. Our results demonstrate that M2 EVs<sup>vMIP-II-Lamp2b</sup> delivered by CTP and PM can promote local myocardial

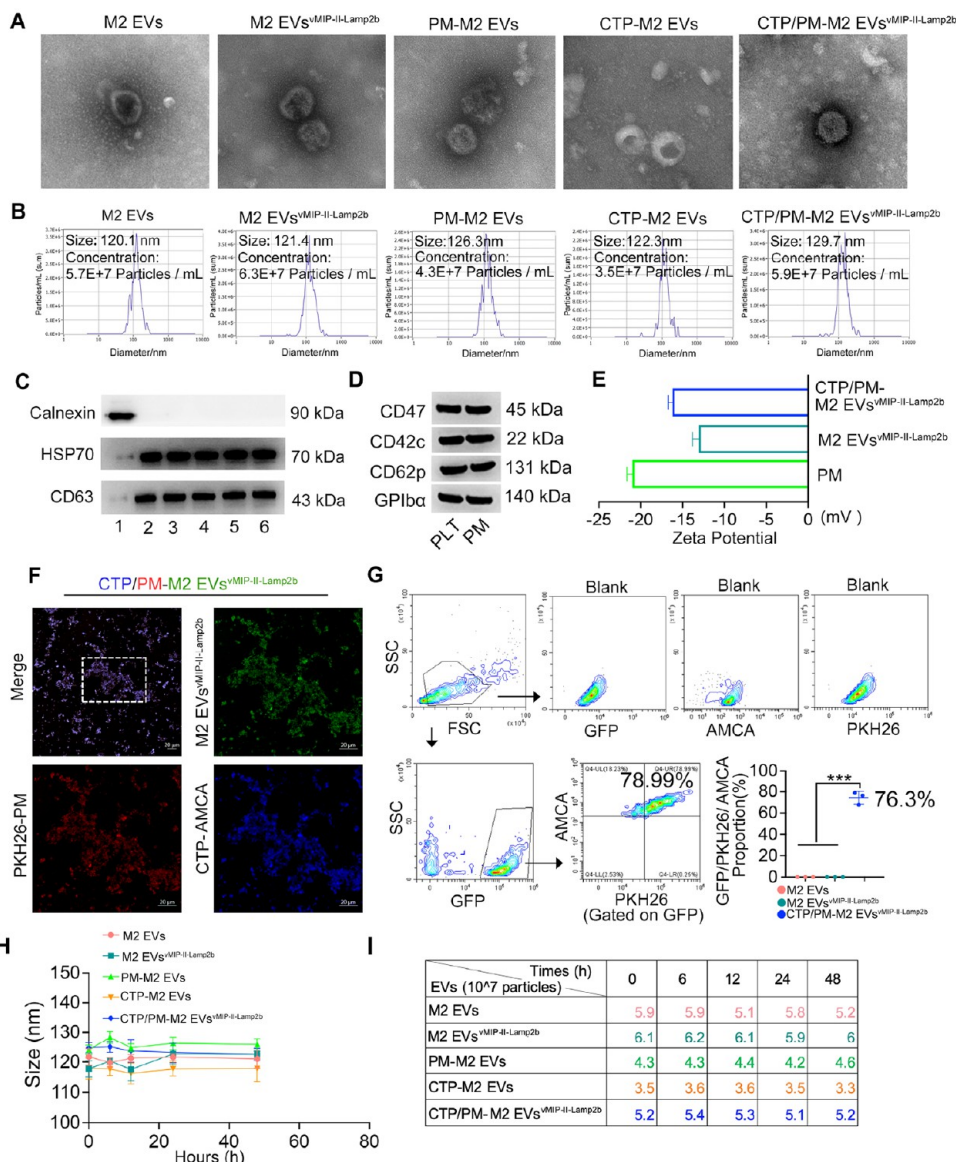


**Figure 1.** Preparation and characterization of CTP/PM-M2 EVs<sup>vMIP-II-Lamp2b</sup>. (A) TEM of M2 EVs, M2 EVs<sup>vMIP-II-Lamp2b</sup>, PM-M2 EVs, CTP-M2 EVs, and CTP/PM-M2 EVs<sup>vMIP-II-Lamp2b</sup>. (B) Nanoparticle tracking analyses (NTA) of M2 EVs, M2 EVs<sup>vMIP-II-Lamp2b</sup>, PM-M2 EVs, CTP-M2 EVs, and CTP/PM-M2 EVs<sup>vMIP-II-Lamp2b</sup>. (C) Western blotting analysis of HSP70, CD63, and calnexin from cells and EVs. 1, 2, 3, 4, 5, and 6 stand for macrophages lysate, M2 EVs, M2 EVs<sup>vMIP-II-Lamp2b</sup>, PM-M2 EVs, CTP-M2 EVs, and CTP/PM-M2 EVs<sup>vMIP-II-Lamp2b</sup>. (D) Western blotting analysis of CD42c, CD47, CD62p, and GPIIbα from PLT and PM. (E) Zeta potential of PM, M2 EVs<sup>vMIP-II-Lamp2b</sup>, and CTP/PM-M2 EVs<sup>vMIP-II-Lamp2b</sup>. (F) Characterization of CTP/PM-M2 EVs<sup>vMIP-II-Lamp2b</sup> under CLSM. CTP was labeled with AMCA, PM was labeled with PKH26, and M2 EVs<sup>vMIP-II-Lamp2b</sup> were green due to the presence of vMIP-II-Lamp2b. (G) Flow cytometry was used to analyze the ratio of CTP, PM, and M2 EVs<sup>vMIP-II-Lamp2b</sup> (representative of similar results obtained from three independent experiments). Results were presented as mean  $\pm$  SEM. \*\*\*  $P < 0.001$  analyzed by one-way ANOVA followed by a multiple-comparison test. (H) Size and number (I) stability of EVs.

immune regulation, inhibit inflammatory reactions, and enhance cardiac repair in mice, thereby illustrating an innovative strategy for the treatment of VM.

## RESULTS AND DISCUSSION

**Identification of M2 Macrophages and Preparation of M2 EVs<sup>vMIP-II-Lamp2b</sup>.** The J774A.1 cells were used to produce sufficient quantities of M0 EVs, M2 EVs, and M2 EVs<sup>vMIP-II-Lamp2b</sup> for all in vitro and in vivo experiments. To generate mock M2 EVs and M2 EVs<sup>vMIP-II-Lamp2b</sup>, mock-Lamp2b-GFP or vMIP-II-Lamp2b-GFP lentivirus was first transfected into J774A.1 cells (Figure S1A) and then polarized

to the M2 phenotype by treating with 20 ng/mL IL-4 and 20 ng/mL IL-13 for 48 h. IL-4- and IL-13-treated J774A.1 cells showed significant upregulation of the M2 macrophages markers Arg-1, YM-1, and FIZZ-1 and downregulation of the M1 macrophages markers iNOS, IL-1 $\beta$ , and TNF- $\alpha$  (Figure S1B). Flow cytometry showed that 99.99% of IL-4- and IL-13-treated J774A.1 cells were CD206<sup>+</sup> and that less than 0.59% were iNOS<sup>+</sup>, indicating successful polarization of J774A.1 cells into the M2 phenotype (Figure S1C). Subsequently, EVs were extracted from vMIP-II-Lamp2b-GFP lentivirus-transfected and IL-4- and IL-13-treated J774A.1 cells (M2 EVs<sup>vMIP-II-Lamp2b</sup>). After incubating M2 EVs<sup>vMIP-II-Lamp2b</sup> with

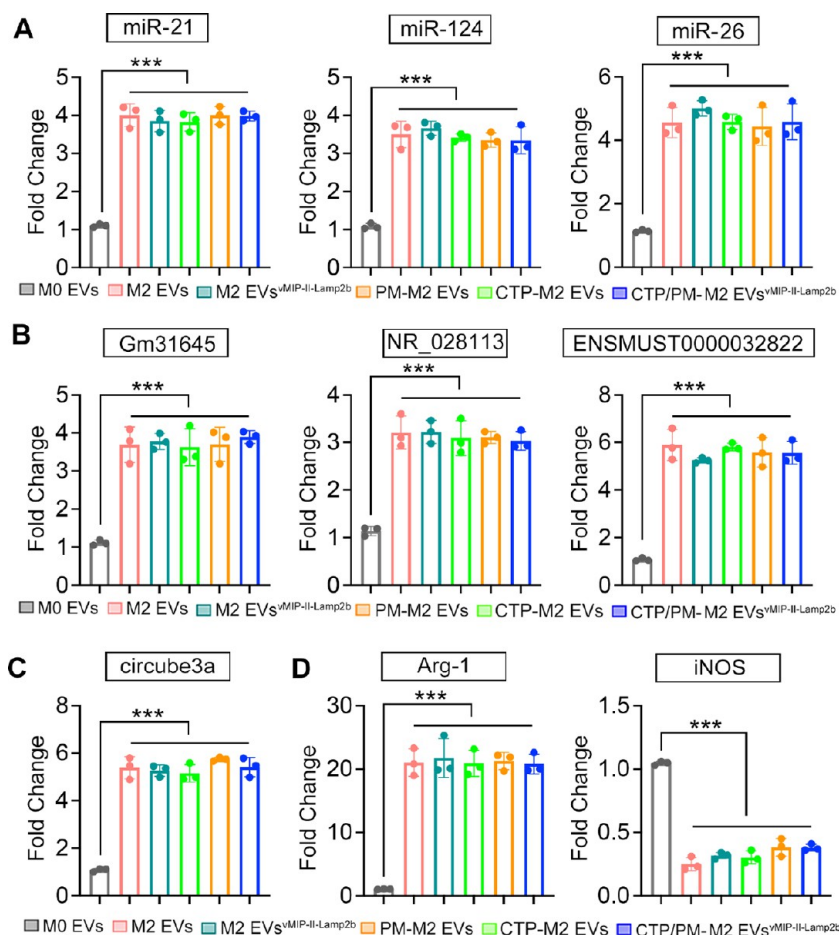


**Figure 2.** NcRNAs and genes expression analysis of EVs. (A) Quantification of three related miRNA expression levels in M0 EVs, M2 EVs, M2-EVs<sup>vMIP-II-Lamp2b</sup>, PM-M2 EVs, CTP-M2 EVs, and CTP/PM-M2 EVs<sup>vMIP-II-Lamp2b</sup> by qRT-PCR. (B) Quantification of three related lncRNA expression levels in M0 EVs, M2 EVs, M2-EVs<sup>vMIP-II-Lamp2b</sup>, PM-M2 EVs, CTP-M2 EVs, and CTP/PM-M2 EVs<sup>vMIP-II-Lamp2b</sup> by qRT-PCR. (C) Quantification of circube3a expression levels in M0 EVs, M2 EVs, M2-EVs<sup>vMIP-II-Lamp2b</sup>, PM-M2 EVs, CTP-M2 EVs, and CTP/PM-M2 EVs<sup>vMIP-II-Lamp2b</sup> by qRT-PCR. (D) Quantification of Arg-1 and iNOS expression levels in M0 EVs, M2 EVs, M2-EVs<sup>vMIP-II-Lamp2b</sup>, PM-M2 EVs, CTP-M2 EVs, and CTP/PM-M2 EVs<sup>vMIP-II-Lamp2b</sup> by qRT-PCR. Results were presented as mean  $\pm$  SEM of three independent experiments. \*\*\*  $P < 0.001$  analyzed by one-way ANOVA followed by a multiple-comparison test.

macrophages for 4 h, GFP green fluorescence was present in the cytoplasm of macrophages, indicating expression of vMIP-II in M2 EVs (Figure S1D). This result was confirmed through Western blotting (Figure S1E), where vMIP-II was found to be highly expressed in M2 EVs<sup>vMIP-II-Lamp2b</sup> compared with M2 EVs. Taken together, these findings demonstrate the successful preparation of M2 EVs<sup>vMIP-II-Lamp2b</sup> to be used for our subsequent experiments.

**Preparation and Characterization of CTP/PM-M2 EVs<sup>vMIP-II-Lamp2b</sup>.** As shown in Figure 1A,B, based on TEM and NTA, M2 EVs, M2 EVs<sup>vMIP-II-Lamp2b</sup>, PM-M2 EVs, CTP-M2 EVs, and CTP/PM-M2 EVs<sup>vMIP-II-Lamp2b</sup> prepared by us exhibited characteristic “round-shaped” morphologies and homogeneous sizes, with peak particle sizes of 120.1, 121.4, 126.3, 122.3, and 129.7 nm, respectively. Using Western blotting (Figure 1C), we further confirmed that all EVs expressed high markers HSP70 and CD63, whereas the negative control cell lysate did not. Additionally, the endoplasmic reticulum marker calnexin was not detected in the EVs. Western blotting also confirmed that the isolated PM still maintained the characteristics of PLT, expressing CD42c, CD47, CD62p, and GPIIb $\alpha$  (Figure 1D). Meanwhile, we measured the zeta potentials of M2 EVs<sup>vMIP-II-Lamp2b</sup> and CTP/

PM-M2 EVs<sup>vMIP-II-Lamp2b</sup> before and after fusion. As shown in Figure 1E, DLS showed that the zeta potential of PM and M2 EVs<sup>vMIP-II-Lamp2b</sup> was  $-20.9$  and  $-13.1$  mV, respectively. CTP/PM-M2 EVs<sup>vMIP-II-Lamp2b</sup> were also negatively charged with a zeta potential of  $-16.2$  mV, which was lower than that of M2 EVs<sup>vMIP-II-Lamp2b</sup> ( $-13.1$  mV). The decreased zeta potential suggested the membrane surface of EVs was changed after the fusion of PM. To further confirm that the M2 EVs<sup>vMIP-II-Lamp2b</sup> were fused with PM and CTP, CTP/PM-M2 EVs<sup>vMIP-II-Lamp2b</sup> were confirmed through observation under CLSM. The M2 EVs<sup>vMIP-II-Lamp2b</sup> “core” appeared green because it was transfected with the vMIP-II-Lamp2b-GFP lentivirus, the PM was labeled with PKH26, and CTP was labeled with AMCA (blue). As shown in Figure 1F, the blue CTP, red membranes, and green EVs exhibited a high degree of colocalization, indicating the successful coating of CTP and PM on M2 EVs<sup>vMIP-II-Lamp2b</sup>. Our flow cytometry results showed that the proportion of triple-positive CTP, PM, and M2 EVs<sup>vMIP-II-Lamp2b</sup> was as high as 76.3% (Figure 1G). At the same time, we also verified the successful preparation of PM-M2 EVs and CTP-M2 EVs by CLSM and FACS. The results showed that CTP or PM and M2 EVs were colocalized, and the proportion of both could reach more than 70% (Figure S2A).

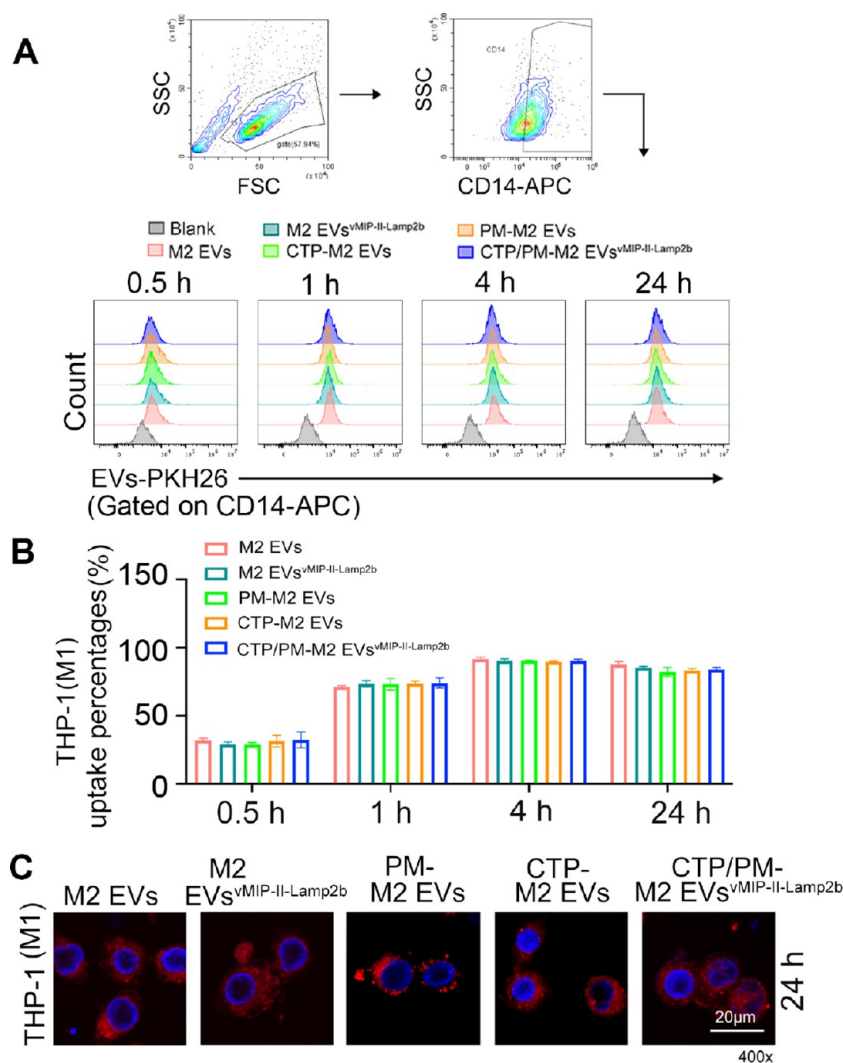


**Figure 3.** Internalization of EVs by THP-1 cells in vitro. (A,B) After M1 macrophages (THP-1) were incubated with M2 EVs, M2 EVs<sup>vMIP-II-Lamp2b</sup>, PM-M2 EVs, CTP-M2 EVs, or CTP/PM-M2 EVs<sup>vMIP-II-Lamp2b</sup> for 24 h, the internalization of EVs was detected by flow cytometry and (C) CLSM. Results were presented as mean  $\pm$  SEM of three independent experiments and analyzed by one-way ANOVA followed by a multiple-comparison test.

To investigate the stability of EVs, M2 EVs, M2 EVs<sup>vMIP-II-Lamp2b</sup>, PM-M2 EVs, CTP-M2 EVs, and CTP/PM-M2 EVs<sup>vMIP-II-Lamp2b</sup> were suspended in 10% mouse serum. The results showed that there was no obvious change in the size and number of EVs within 48 h (Figure 1H,I). Surprisingly, the number of EVs did not decrease significantly over time. Simultaneously, CTP/PM-M2 EVs<sup>vMIP-II-Lamp2b</sup> were coincubated with macrophages for 3 days, and the expression of green fluorescence in macrophages was detected at different time points. As shown in Figure S2B, vMIP-II was persistent in M2 EVs.

Next, we evaluated the cytotoxicity of several types of EVs in vitro, and BMDMs were treated with M2 EVs, M2 EVs<sup>vMIP-II-Lamp2b</sup>, PM-M2 EVs, CTP-M2 EVs, or CTP/PM-M2 EVs<sup>vMIP-II-Lamp2b</sup>. After 4 h of incubation, cells were collected for apoptosis detection by flow cytometry. The results in Figure S2C showed that compared with PBS, all EVs had no obvious toxic effect on BMDMs, indicating the safety of the EVs used.

**Noncoding RNAs (ncRNAs) Expression in EVs.** It has been reported that EVs modulate the function of recipient cells

by delivering their bioactive components, especially ncRNAs.<sup>28–30</sup> Therefore, to better understand the key ncRNAs of M2 EVs involved in immune regulation, we performed tests in M2 EVs, M2 EVs<sup>vMIP-II-Lamp2b</sup>, PM-M2 EVs, CTP-M2 EVs, and CTP/PM-M2 EVs<sup>vMIP-II-Lamp2b</sup> based on previously reported relevant ncRNAs to assess the content integrity of engineered CTP/PM-M2 EVs<sup>vMIP-II-Lamp2b</sup>. In previous studies, miR-21,<sup>31,32</sup> miR-124,<sup>33,34</sup> and miR-26<sup>35</sup> have been reported to play an important role in M2 macrophages regulation, and our results show that these miRNAs in M2 EVs, M2 EVs<sup>vMIP-II-Lamp2b</sup>, PM-M2 EVs, CTP-M2 EVs, and CTP/PM-M2 EVs<sup>vMIP-II-Lamp2b</sup> are approximately 3~5-fold more abundant than those in M0 EVs (Figure 2A). For lncRNAs, we also screened three lncRNAs according to the sequencing results in the database (GSA: CRA009657). Gm31645, NR\_028113, and ENSMUST0000032822 were highly expressed in all M2 EV groups (Figure 2B). Similarly, this expression trend was also reflected in circube3a,<sup>30</sup> a circRNA associated with M2 macrophages (Figure 2C). In parallel, the M2-related gene Arg-1 and the M1-related gene iNOS were also detected. As shown in Figure 2D, compared

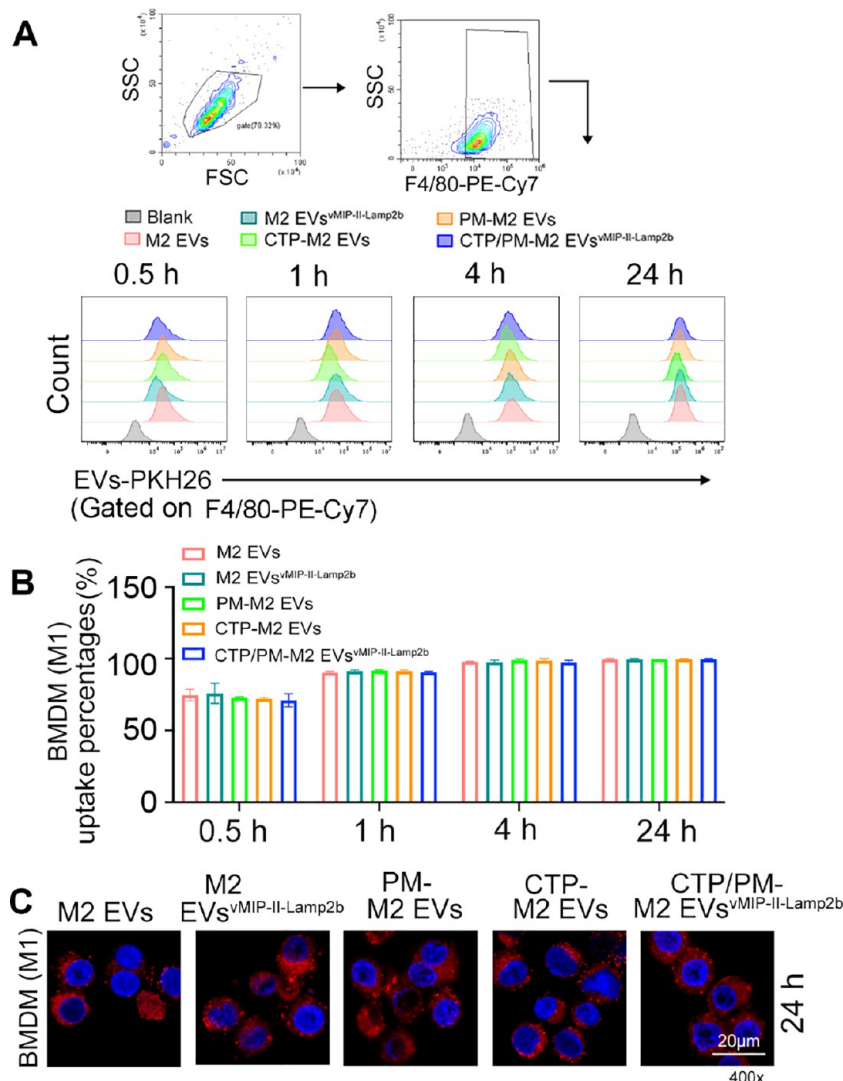


**Figure 4.** Internalization of EVs by BMDMs in vitro. (A,B) After M1 macrophages (BMDMs) were incubated with M2 EVs, M2 EVs<sup>vMIP-II-Lamp2b</sup>, PM-M2 EVs, CTP-M2 EVs, or CTP/PM-M2 EVs<sup>vMIP-II-Lamp2b</sup> for 24 h, the internalization of EVs was detected by flow cytometry and (C) CLSM. Results were presented as mean  $\pm$  SEM of three independent experiments and analyzed by one-way ANOVA followed by a multiple-comparison test.

with M0 EVs, Arg-1 was highly expressed in M2 EVs, M2 EVs<sup>vMIP-II-Lamp2b</sup>, PM-M2 EVs, CTP-M2 EVs, and CTP/PM-M2 EVs<sup>vMIP-II-Lamp2b</sup>, while iNOS expression was decreased. In summary, the various engineered M2 EV contents prepared by us were not damaged. In particular, CTP/PM-M2 EVs<sup>vMIP-II-Lamp2b</sup> can release these beneficial ncRNAs and genes when they reach heart tissues, thus having the potential to relieve myocardial inflammation.

#### Internalization and Cargo Transport of EVs in Vitro.

Ly6C monocytes preferentially differentiate into M1 macrophages in the inflamed myocardium; therefore, we first tested whether CTP/PM-M2 EVs<sup>vMIP-II-Lamp2b</sup> could be internalized by activated monocytes in vitro. To this end, THP-1 monocytes were pretreated with LPS and IFN- $\gamma$ , before incubating with PKH26-labeled M2 EVs, M2 EVs<sup>vMIP-II-Lamp2b</sup>, PM-M2 EVs, CTP-M2 EVs, and CTP/PM-M2 EVs<sup>vMIP-II-Lamp2b</sup> for 0.5, 1, 4, and 24 h. As shown in Figure 3A,B, after incubation for 0.5 h, the proportion of THP-1-differentiated macrophages internalizing M2 EVs, M2 EVs<sup>vMIP-II-Lamp2b</sup>, PM-M2 EVs, CTP-M2 EVs, and CTP/PM-M2 EVs<sup>vMIP-II-Lamp2b</sup> ranged from 30.47 to 38.97%. After 1 h,

the proportion of their internalization by macrophages increased significantly with time and the percentage of internalization increased by more than 72%. The internalization rate of EVs reached a peak of more than 89% at 4 h, and the internalization proportion increased by 50% compared to 30 min. After 24 h, the internalization effect of the five EVs decreased slightly but still remained above 80%. At the same time, we confirmed the presence of a large number of EVs in the cytoplasm of THP-1 cells at 24 h by CLSM (Figure 3C).

We also differentiated bone-marrow-derived macrophages (BMDM) into M1 macrophages and incubated them with PKH26-labeled M2 EVs, M2 EVs<sup>vMIP-II-Lamp2b</sup>, PM-M2 EVs, CTP-M2 EVs, and CTP/PM-M2 EVs<sup>vMIP-II-Lamp2b</sup> for 0.5, 1, 4, and 24 h. As shown in Figure 4, M1 macrophages had internalized more EVs after incubation for 0.5 h, with the internalization proportion as high as approximately 66%, far exceeding that of THP-1-differentiated macrophages at 0.5 h. Over time, the proportion of M1 macrophages that internalized EVs remained stable. At 24 h, the internalization ratio remained at approximately 99%, which was approximately

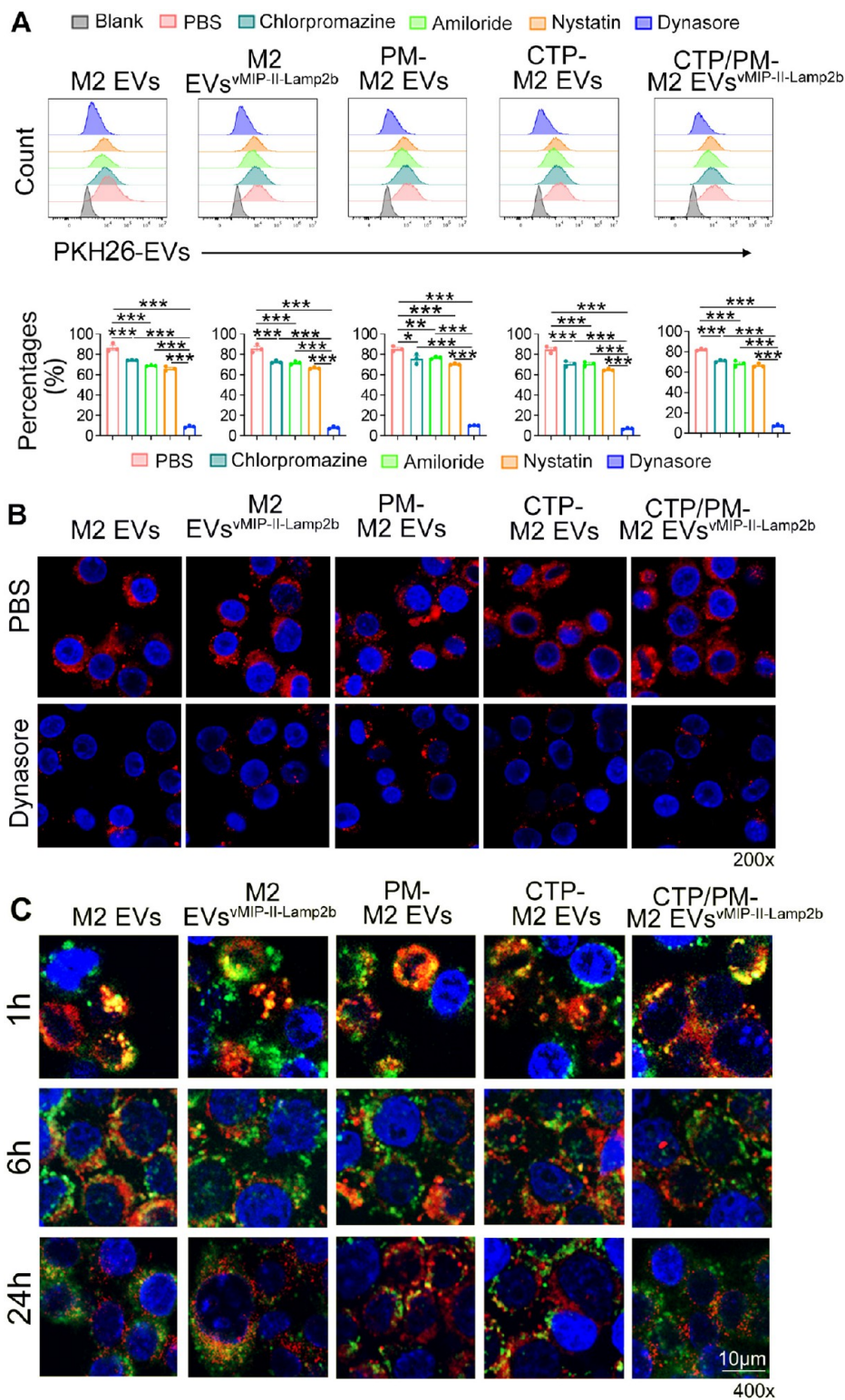


**Figure 5.** Mechanism of internalization of EVs. (A) Flow cytometry analysis and quantification of PKH26-labeled M2 EVs, M2 EVs<sup>vMIP-II-Lamp2b</sup>, PM-M2 EVs, CTP-M2 EVs, or CTP/PM-M2 EVs<sup>vMIP-II-Lamp2b</sup> (red) by M1 macrophages under different endocytic inhibitors. (B) Representative confocal images of PKH26-labeled M2 EVs, M2 EVs<sup>vMIP-II-Lamp2b</sup>, PM-M2 EVs, CTP-M2 EVs, or CTP/PM-M2 EVs<sup>vMIP-II-Lamp2b</sup> were internalized by M1 macrophages under Dynasore (dynamic dependent endocytosis inhibitor). (C) Representative confocal images of PKH26-labeled M2 EVs, M2 EVs<sup>vMIP-II-Lamp2b</sup>, PM-M2 EVs, CTP-M2 EVs, or CTP/PM-M2 EVs<sup>vMIP-II-Lamp2b</sup> (red) in M1 macrophages stained with LysoTracker (green: lysosomes). Yellow color represented colocalization of fluorescent signals from EVs and lysosomes. (Note: M2 EVs<sup>vMIP-II-Lamp2b</sup> and CTP/PM-M2 EVs<sup>vMIP-II-Lamp2b</sup> used here are GFP-free). Results were presented as mean  $\pm$  SEM of three independent experiments. \* $P < 0.05$ ; \*\* $P < 0.01$ ; \*\*\* $P < 0.001$  analyzed by one-way ANOVA followed by a multiple-comparison test.

15% higher than that of the THP-1-differentiated macrophages.

Next, we explored the mechanism of internalization of these EVs. Macrophages were pretreated with different endocytosis inhibitors (Dynasore: dynamic dependent endocytosis inhibitor; amiloride: macropinocytosis inhibitor; nystatin: fassa protein-mediated endocytosis inhibitor; and chlorpromazine: clathrin-mediated endocytosis inhibitor) and then cultured with EVs for 1 h. The results showed that the internalization of M2 EVs, M2 EVs<sup>vMIP-II-Lamp2b</sup>, PM-M2 EVs, CTP-M2 EVs, and CTP/PM-M2 EVs<sup>vMIP-II-Lamp2b</sup> was mainly suppressed by Dynasore (dynamic dependent endocytosis inhibitor). Dynasore inhibited about 90% of EVs internalized by macrophages, which was more than that of other inhibitors (approximately 30%) (Figure 5A). The results of CLSM further confirm this (Figure 5B). These suggest that these EVs are endocytosed mainly through a dynamically dependent pathway.

Macrophages, as phagocytes, contain a large number of lysosomes,<sup>36</sup> so it is critical to evaluate the lysosomal escape capacity of EVs in macrophages. We assessed the escape capacity of each EV in the lysosomal compartment at different time points, and we stained the lysosomes with a lysosomal tracker (green). Within the first hour after internalization, we found that all EVs were all trapped in lysosomes. After 6 h, the signals of PKH26 (Red) and lysosomes were partially separated, indicating that EVs were escaping from lysosomes. After 24 h, the signals were completely separated, indicating that EVs began to escape successfully (Figure 5C).

To further test whether CTP/PM-M2 EVs<sup>vMIP-II-Lamp2b</sup> successfully delivered ncRNAs into macrophages, we examined the relevant ncRNA expression levels in macrophages. As shown in Figure S3, the expression levels of miR-21, miR-124, miR-26, Gm31645, NR\_028113, ENSMUST0000032822, and circube3a in M1 macrophages after incubation with CTP/PM-M2 EVs<sup>vMIP-II-Lamp2b</sup> were significantly increased compared with those in M1 macrophages before incubation with CTP/PM-M2 EVs<sup>vMIP-II-Lamp2b</sup>. Overall, CTP/PM-M2 EVs<sup>vMIP-II-Lamp2b</sup> show further potential to reprogram macrophages by delivering ncRNAs.

**Immunoregulation of CTP/PM-M2 EVs<sup>vMIP-II-Lamp2b</sup> in Vitro.** To explore the immunomodulatory effect of CTP/PM-M2 EVs<sup>vMIP-II-Lamp2b</sup>, we treated M1 macrophages (BMDMs) with M2 EVs, M2 EVs<sup>vMIP-II-Lamp2b</sup>, PM-M2 EVs, CTP/PM-M2 EVs, or CTP/PM-M2 EVs<sup>vMIP-II-Lamp2b</sup> and then performed flow cytometry analysis and qRT-PCR to detect the macrophage polarization status and chemokine receptor change levels. The results of flow cytometry showed that after 24 h of treatment, the proportion of M1 macrophages in the M2 EVs, M2 EVs<sup>vMIP-II-Lamp2b</sup>, PM-M2 EVs, CTP-M2 EVs, and CTP/PM-M2 EVs<sup>vMIP-II-Lamp2b</sup> groups was 38.52, 35.14, 35.28, 37.41, and 33.53%, respectively, while that of M2 macrophages was 50.83, 54.56, 52.15, 52.92, and 60.05%, respectively (Figure 6A). After statistical analysis (Figure 6C), it is worth noting that M2 EVs<sup>vMIP-II-Lamp2b</sup> and CTP/PM-M2 EVs<sup>vMIP-II-Lamp2b</sup> can promote the polarization of M1 macrophages to M2 better than the other three groups in vitro. After 24 h incubation of M1 macrophages with EVs, the proportion of F4/80<sup>+</sup>CD206<sup>+</sup> was highest in the CTP/PM-M2 EVs<sup>vMIP-II-Lamp2b</sup> group, exceeding that in the M2 EVs, PM-M2 EVs, and CTP-M2 EVs groups. Compared with 24 h, the proportion of M2 macrophages in the M2 EVs, M2 EVs<sup>vMIP-II-Lamp2b</sup>, PM-M2 EVs, CTP-M2 EVs, and CTP/PM-M2 EVs<sup>vMIP-II-Lamp2b</sup> groups increased by approximately 37, 41, 45, 40, and 28% at 48 h,

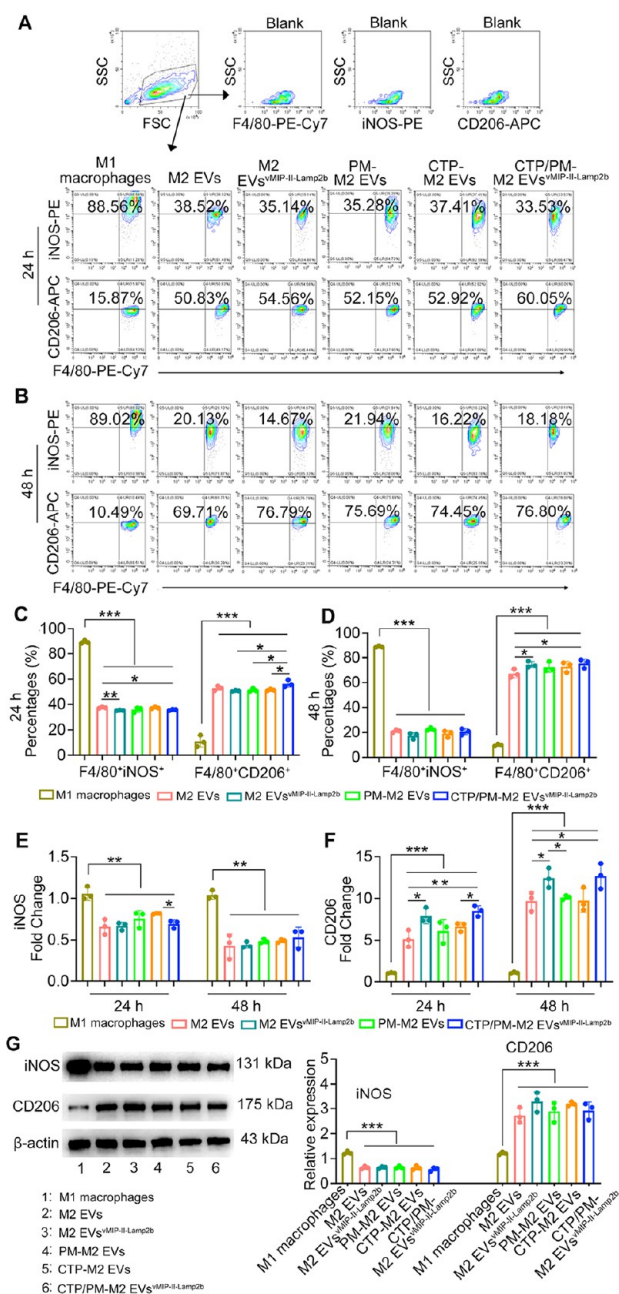


**Figure 6.** Immunoregulation of CTP/PM-M2 EVs<sup>vMIP-II-Lamp2b</sup> in vitro. BMDMs were stimulated to M1 macrophages and then incubated with M2 EVs, M2-EVs<sup>vMIP-II-Lamp2b</sup>, PM-M2 EVs, CTP-M2 EVs, and CTP/PM-M2 EVs<sup>vMIP-II-Lamp2b</sup> for 24 and 48 h. M1 macrophages were used as control. (A) Representative flow cytometry plots of M1 macrophages (F4/80<sup>+</sup>/iNOS<sup>+</sup>) and M2 macrophages (F4/80<sup>+</sup>/CD206<sup>+</sup>) were detected at 24 h. (B) Representative flow cytometry plots of M1 macrophages (F4/80<sup>+</sup>/iNOS<sup>+</sup>) and M2 macrophages (F4/80<sup>+</sup>/CD206<sup>+</sup>) were detected at 48 h. (C) A bar graph of macrophage percentages in figure A. (D) A bar graph of macrophage percentages in figure B. (E) Quantification of iNOS mRNA expression in macrophages by qRT-PCR at 24 and 48 h. (F) Quantification of CD206 mRNA expression in macrophages by qRT-PCR at 24 and 48 h. (G) Quantification of iNOS and CD206 protein expression in macrophages by Western blotting at 48 h. Results were presented as mean  $\pm$  SEM of three independent experiments. \* $P$  < 0.05; \*\* $P$  < 0.01; \*\*\* $P$  < 0.001 analyzed by one-way ANOVA followed by a multiple-comparison test.

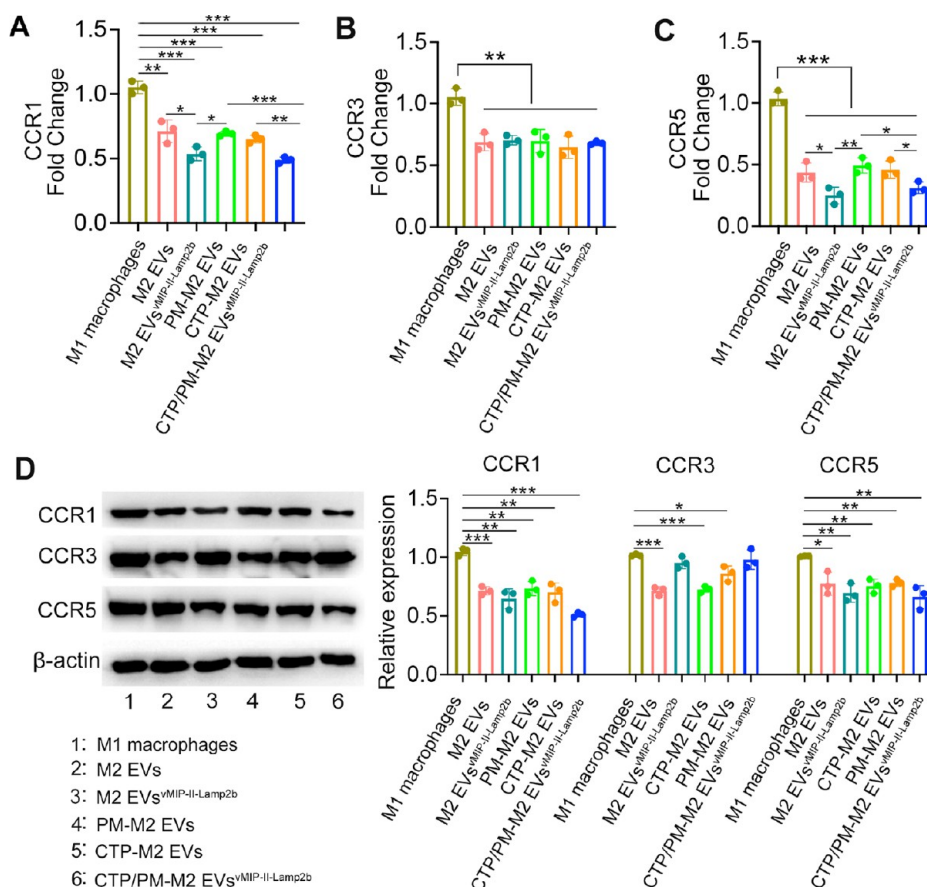


**Figure 7.** Immunoregulation of CTP/PM-M2 EVs<sup>vMIP-II-Lamp2b</sup> in vitro. BMDMs were stimulated to M1 macrophages and then incubated with M2 EVs, M2 EVs<sup>vMIP-II-Lamp2b</sup>, PM-M2 EVs, CTP-M2 EVs, and CTP/PM-M2 EVs<sup>vMIP-II-Lamp2b</sup> for 48 h. Quantification of CCR1 (A), CCR3 (B), and CCR5 (C) mRNA expression in M1 macrophages by qRT-PCR. (D) Quantification of CCR1, CCR3, and CCR5 protein expression in M1 macrophages by Western blotting. Results were presented as mean  $\pm$  SEM of three independent experiments. \* $P < 0.05$ ; \*\* $P < 0.01$ ; \*\*\* $P < 0.001$  analyzed by one-way ANOVA followed by a multiple-comparison test.

respectively (Figure 6B), indicating that the reprogramming ability of M2 EVs was excellent. Meanwhile, our qRT-PCR results also showed that compared with M1 macrophages at 24 h, the mRNA expression of CD206 was significantly increased in the M2 EVs<sup>vMIP-II-Lamp2b</sup> (~7.5-fold, vs the M1 macrophages group) and CTP/PM-M2 EVs<sup>vMIP-II-Lamp2b</sup> (~8.0-fold, vs the M1 macrophages group)-treated groups, which was accompanied by decreased mRNA expression of iNOS (Figure 6E). The qRT-PCR results were similar to those of flow cytometry, and the mRNA level of the M2 marker was increased after 48 h compared with that at 24 h (Figure 6F). Western blotting analysis showed that M2 EVs, M2 EVs<sup>vMIP-II-Lamp2b</sup>, PM-M2 EVs, CTP/PM-M2 EVs, and CTP/PM-M2 EVs<sup>vMIP-II-Lamp2b</sup> treatment of M1 macrophages for 48 h significantly inhibited the expression of iNOS and upregulated the expression of CD206 (Figure 6G). Taken together, we found that M2 EVs, M2 EVs<sup>vMIP-II-Lamp2b</sup>, PM-M2 EVs, CTP/PM-M2 EVs, and CTP/PM-M2 EVs<sup>vMIP-II-Lamp2b</sup>, especially M2 EVs<sup>vMIP-II-Lamp2b</sup> and CTP/PM-M2 EVs<sup>vMIP-II-Lamp2b</sup>, displayed immunoregulatory effects.

The regulatory ability of EVs was also reflected in the expression of chemokine receptors. After M1 macrophages were incubated with EVs for 48 h, the mRNA and protein levels of chemokine receptors were detected by qRT-PCR and Western blotting. As shown in Figure 7A–C, the mRNA expression levels of CCR1, CCR3, and CCR5 were decreased

in M1 macrophages treated with M2 EVs, M2 EVs<sup>vMIP-II-Lamp2b</sup>, PM-M2 EVs, CTP-M2 EVs, and CTP/PM-M2 EVs<sup>vMIP-II-Lamp2b</sup>. Specifically, compared with the other three groups (M2 EVs, PM-M2 EVs, and CTP-M2 EVs), M2 EVs<sup>vMIP-II-Lamp2b</sup> and CTP/PM-M2 EVs<sup>vMIP-II-Lamp2b</sup> significantly downregulated the mRNA expression levels of chemokine receptors (CCR1 and CCR5). Although the expression of CCR3 was lower than that of the other three groups, it did not produce statistical significance. Furthermore, Western blotting results (Figure 7D) also showed that the protein levels of CCR1, CCR3, and CCR5 in M1 macrophages were significantly decreased after EVs treatment. M2 EVs<sup>vMIP-II-Lamp2b</sup> and CTP/PM-M2 EVs<sup>vMIP-II-Lamp2b</sup> also demonstrated their inhibitory advantages on the protein expression levels of CCR1 and CCR5. Unfortunately, the immunomodulatory advantages of M2 EVs<sup>vMIP-II-Lamp2b</sup> and CTP/PM-M2 EVs<sup>vMIP-II-Lamp2b</sup> were not reflected in CCR3.

In conclusion, M2 EVs, M2 EVs<sup>vMIP-II-Lamp2b</sup>, PM-M2 EVs, CTP-M2 EVs, and CTP/PM-M2 EVs<sup>vMIP-II-Lamp2b</sup> can promote the polarization of M1 macrophages to M2 in vitro, thereby exerting immunomodulatory effects, and the regulatory effect of M2 EVs<sup>vMIP-II-Lamp2b</sup> and CTP/PM-M2 EVs<sup>vMIP-II-Lamp2b</sup> is relatively superior.

**Biodistribution and Targeting Ability of CTP/PM-M2 EVs<sup>vMIP-II-Lamp2b</sup> in Vivo.** Having determined the function of EVs in M1 macrophages in vitro, we next sought to track the

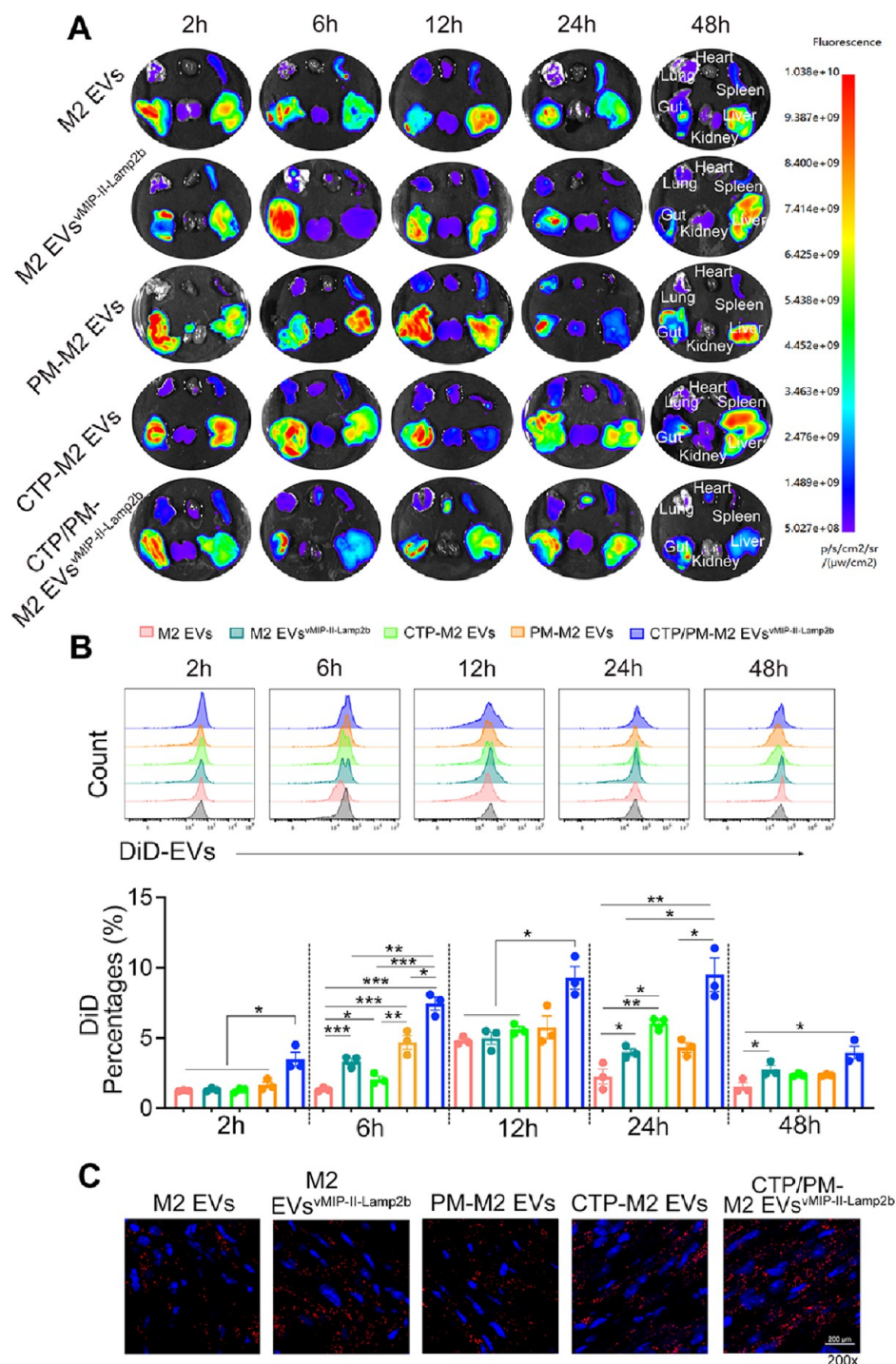


**Figure 8.** Biodistribution of CTP/PM-M2 EVs<sup>vMIP-II-Lamp2b</sup> in vivo. (A) Ex vivo image of organs (heart, liver, spleen, kidney, gut, and lung) post injection with DiD-labeled M2 EVs, M2 EVs<sup>vMIP-II-Lamp2b</sup>, PM-M2 EVs, CTP-M2 EVs, or CTP/PM-M2 EVs<sup>vMIP-II-Lamp2b</sup> in VM mice ( $n = 3$  mice/per group). (B) The proportion of DiD-labeled M2 EVs, M2 EVs<sup>vMIP-II-Lamp2b</sup>, PM-M2 EVs, CTP-M2 EVs, or CTP/PM-M2 EVs<sup>vMIP-II-Lamp2b</sup> in the heart tissues was analyzed by flow cytometry ( $n = 3$  mice/per group). (C) Representative images of DiD-labeled M2 EVs, M2 EVs<sup>vMIP-II-Lamp2b</sup>, PM-M2 EVs, CTP-M2 EVs, or CTP/PM-M2 EVs<sup>vMIP-II-Lamp2b</sup> in heart tissues of VM mice. Results were presented as mean  $\pm$  SEM. \* $P < 0.05$ ; \*\* $P < 0.01$ ; \*\*\* $P < 0.001$  analyzed by one-way ANOVA followed by a multiple-comparison test.

biodistribution of EVs in vivo. To this end, DiD-labeled M2 EVs, M2 EVs<sup>vMIP-II-Lamp2b</sup>, PM-M2 EVs, CTP/PM-M2 EVs, or CTP/PM-M2 EVs<sup>vMIP-II-Lamp2b</sup> were injected into VM mice via the tail vein on days 3. The in vivo imaging system (IVIS) images (Figure 8A) revealed that the duration of DiD in VM mice could exceed 48 h. As controls, DiD-labeled M2 EVs, M2 EVs<sup>vMIP-II-Lamp2b</sup>, PM-M2 EVs, and CTP-M2 EVs showed in

vivo biodistribution similar to DiD-labeled CTP/PM-M2 EVs<sup>vMIP-II-Lamp2b</sup>. They were distributed in the liver, spleen, kidney, lung, gut, and heart. We measured the proportion of EVs in the above organs at different time points by flow cytometry (Figures 8B and S4). The accumulation of these EVs in the liver and gut was significantly more than that in other organs and tissues (Figure S4D,4E). The ex vivo imaging

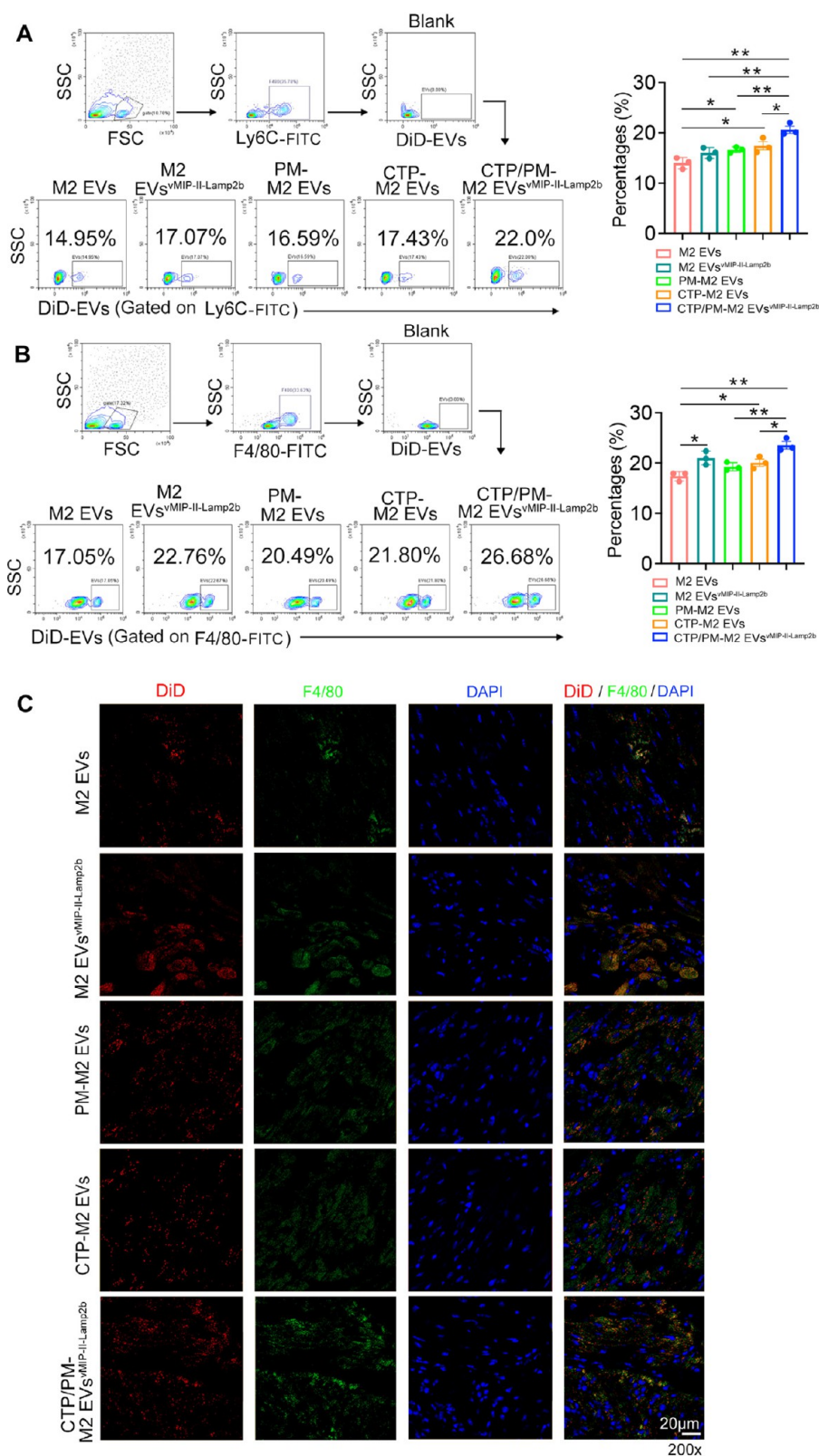


**Figure 9.** Targeting ability of CTP/PM-M2 EVs<sup>vMIP-II-Lamp2b</sup> *in vivo*. (A) Percentages of DiD-EVs targeted Ly6C<sup>+</sup> monocytes in the heart tissues ( $n = 5$  mice/per group). (B) Percentages of DiD-EVs targeted F4/80<sup>+</sup> monocytes in the heart tissues ( $n = 5$  mice/per group). (C) Representative confocal images of DiD-labeled M2 EVs, M2 EVs<sup>vMIP-II-Lamp2b</sup>, PM-M2 EVs, CTP-M2 EVs, or CTP/PM-M2 EVs<sup>vMIP-II-Lamp2b</sup> (red) colocalized with F4/80<sup>+</sup> (green) macrophages in the heart tissues ( $n = 3$  mice/per group). (Note: M2 EVs<sup>vMIP-II-Lamp2b</sup> and CTP/PM-M2 EVs<sup>vMIP-II-Lamp2b</sup> used here are GFP-free). Results were presented as mean  $\pm$  SEM of three independent experiments. \* $P < 0.05$ ; \*\* $P < 0.01$ ; \*\*\* $P < 0.001$  analyzed by one-way ANOVA followed by a multiple-comparison test.

of organs displayed that at 2 h, CTP/PM-M2 EVs<sup>vMIP-II-Lamp2b</sup> appeared in the heart with visible fluorescence and displayed significantly more accumulation (approximately 3%) than all control groups (approximately 1%). Over time, more and more EVs begin to enter the heart. At 6 h, the level of accumulation of CTP/PM-M2 EVs<sup>vMIP-II-Lamp2b</sup> in the hearts of VM mice reached approximately 7.4%. From 12 to 24 h, the accumulation of EVs in control groups reached a peak, while the accumulation of CTP/PM-M2 EVs<sup>vMIP-II-Lamp2b</sup> (approximately 7%) in the heart was still higher than that in others. From 24 to 48 h, the EVs in the heart of each group were reduced, but visible fluorescence was still present in the CTP/PM-M2 EVs<sup>vMIP-II-Lamp2b</sup> group. This is because unmodified EVs that enter the blood circulation through tail vein injection are easily retained by organs such as the liver and spleen, resulting in a high distribution of EVs in these areas, which, in turn, reduces the number of EVs reaching the target organs. As shown in Figure S4A,D, the proportion of DiD-labeled CTP/PM-M2 EVs<sup>vMIP-II-Lamp2b</sup> in the liver and spleen was less than other control EVs at 6 and 12 h, but no significant difference was seen in other organs. As the fluorescence intensity of the heart was the strongest at 24 h, DiD-labeled M2 EVs, M2 EVs<sup>vMIP-II-Lamp2b</sup>, PM-M2 EVs, CTP-M2 EVs, or CTP/PM-M2 EVs<sup>vMIP-II-Lamp2b</sup> were injected intravenously into the VM mice on days 3, and the hearts were removed 24 h later for frozen sections. The CLSM results show that the CTP/PM-M2 EVs<sup>vMIP-II-Lamp2b</sup> were considerably more concentrated in the hearts than M2 EVs, M2 EVs<sup>vMIP-II-Lamp2b</sup>, PM-M2 EVs, and CTP-M2 EVs (Figure 8C). These results suggest that the PM and CTP decoration of M2 EVs<sup>vMIP-II-Lamp2b</sup> significantly promotes their accumulation in hearts and therefore improves the expected therapeutic effect.

As CTP/PM-M2 EVs<sup>vMIP-II-Lamp2b</sup> could be delivered to hearts, we next sought to investigate whether they could target monocytes and macrophages in the hearts. Flow cytometry analysis showed that the proportions of DiD-labeled M2 EVs, M2 EVs<sup>vMIP-II-Lamp2b</sup>, PM-M2 EVs, CTP-M2 EVs in monocytes were 14.95, 17.07, 16.59, and 17.43%, respectively, lower than that of CTP/PM-M2 EVs<sup>vMIP-II-Lamp2b</sup> (22%) (Figure 9A). We then examined the ability of cardiac macrophages to bind to EVs. As shown in Figure 9B, DiD-labeled CTP/PM-M2 EVs<sup>vMIP-II-Lamp2b</sup> in F4/80 macrophages in the hearts (26.68%) were also higher than the M2 EVs (17.05%), M2 EVs<sup>vMIP-II-Lamp2b</sup> (22.76%), PM-M2 EVs (20.49%), and CTP-M2 EVs (21.80%) treatment groups. The confocal immunofluorescence image of the hearts also showed that more DiD-labeled CTP/PM-M2 EVs<sup>vMIP-II-Lamp2b</sup> gathered in the hearts and colocalized with F4/80 macrophages (Figure 9C). In summary, we demonstrated that CTP/PM-M2 EVs<sup>vMIP-II-Lamp2b</sup> could be endocytosed in monocytes and cardiac macrophages, which is necessary for further treatment.

**Immunoregulation of CTP/PM-M2 EVs<sup>vMIP-II-Lamp2b</sup> in Vivo.** Previous studies have demonstrated that M1 macrophages are major drivers of VM progression.<sup>7–9</sup> M1 macrophages typically exhibit proinflammatory functions in the immune microenvironment, while M2 macrophages exhibit anti-inflammatory functions. M1 and M2 macrophages coexist within the heart tissue, and the ratio of M1/M2 subsets directly affects the immune response to VM. As our previous experiments confirmed that M2 EVs can be internalized by macrophages in the heart, we next sought to investigate whether the uptake of CTP/PM-M2 EVs<sup>vMIP-II-Lamp2b</sup> can reprogram macrophages into M2 macrophages in vivo, thus

regulating the cardiac immune microenvironment in a favorable direction. To optimize experimental grouping, VM mice were treated in the following four groups, PBS, M2 EVs, M2 EVs<sup>vMIP-II-Lamp2b</sup>, and CTP/PM-M2 EVs<sup>vMIP-II-Lamp2b</sup>. The hearts of VM mice were collected 48 h after the last administration, and a single-cell suspension was prepared for flow cytometry, qRT-PCR, and Western blotting analysis. As shown in Figure 10A–D, compared with the PBS treatment group, M2 EVs, M2 EVs<sup>vMIP-II-Lamp2b</sup>, and CTP/PM-M2 EVs<sup>vMIP-II-Lamp2b</sup> decreased the population of M1 macrophages and increased M2 macrophages in the heart tissues. However, the CTP/PM-M2 EVs<sup>vMIP-II-Lamp2b</sup> treatment worked best for M1 macrophage reprogramming in VM mice. Compared with the PBS treatment group, M1 macrophages decreased by approximately 16, 30, and 35% after M2 EVs, M2 EVs<sup>vMIP-II-Lamp2b</sup>, and CTP/PM-M2 EVs<sup>vMIP-II-Lamp2b</sup> treatment, respectively, while M2 macrophages increased by approximately 32, 48, and 70%, respectively. Similar results were confirmed using qRT-PCR, in that, compared with PBS, the mRNA expression of iNOS in the hearts of VM mice after M2 EVs, M2 EVs<sup>vMIP-II-Lamp2b</sup>, and CTP/PM-M2 EVs<sup>vMIP-II-Lamp2b</sup> treatment was downregulated by approximately 20, 40, and 50%, respectively, while the M2-related gene (CD206) was upregulated by approximately 2.5-, 3.3-, and 4.1-fold, respectively (Figure 10E,F). The protein expression of iNOS and CD206 in VM mice treated with CTP/PM-M2 EVs<sup>vMIP-II-Lamp2b</sup> showed similar results to qRT-PCR, and CTP/PM-M2 EVs<sup>vMIP-II-Lamp2b</sup> could significantly downregulate the protein expression of iNOS and upregulate CD206 (Figure 10G,H). Furthermore, we measured the expression of the inflammatory cytokines TNF- $\alpha$ , IFN- $\gamma$ , IL-4, and TGF- $\beta$  in heart tissues. The results showed that CTP/PM-M2 EVs<sup>vMIP-II-Lamp2b</sup> could downregulate the levels of IFN- $\gamma$  and upregulate the levels of TGF- $\beta$  more effectively than M2 EVs and M2 EVs<sup>vMIP-II-Lamp2b</sup>. The levels of TNF- $\alpha$  decreased but without statistical significance; however, compared with PBS, CTP/PM-M2 EVs<sup>vMIP-II-Lamp2b</sup> significantly downregulated TNF- $\alpha$  expression. Similarly, we found that IL-4 was not upregulated significantly after CTP/PM-M2 EVs<sup>vMIP-II-Lamp2b</sup> treatment compared with M2 EVs and M2 EVs<sup>vMIP-II-Lamp2b</sup> treatment but was upregulated in the heart compared with PBS (Figure 10I,L). Meanwhile, macrophages isolated from VM mice treated with PBS produced a large amount of NO compared with those isolated from VM mice treated with M2 EVs, M2 EVs<sup>vMIP-II-Lamp2b</sup>, or CTP/PM-M2 EVs<sup>vMIP-II-Lamp2b</sup>. However, NO levels were not significantly different among M2 EVs, M2 EVs<sup>vMIP-II-Lamp2b</sup>, and CTP/PM-M2 EVs<sup>vMIP-II-Lamp2b</sup> groups (Figure S5A).

Next, we detected changes in the mRNA and protein levels of the chemokine receptors. The results showed that the mRNA levels of CCR1, CCR3, and CCR5 were significantly decreased after CTP/PM-M2 EVs<sup>vMIP-II-Lamp2b</sup> treatment compared with those in the PBS-treated group (Figure 10M–O). Compared with M2 EVs, M2 EVs carrying vMIP-II (M2 EVs<sup>vMIP-II-Lamp2b</sup> and CTP/PM-M2 EVs<sup>vMIP-II-Lamp2b</sup>) significantly downregulated the expression of CCR1 and CCR5 but not CCR3. This indicated that vMIP-II not only helps to increase the targeting ability of M2 EVs but also downregulates the expression of chemokine receptors in the inflammatory environment. We found similar results for changes in protein levels; specifically, CTP/PM-M2 EVs<sup>vMIP-II-Lamp2b</sup> treatment downregulated the protein expression levels of CCR1, CCR3,

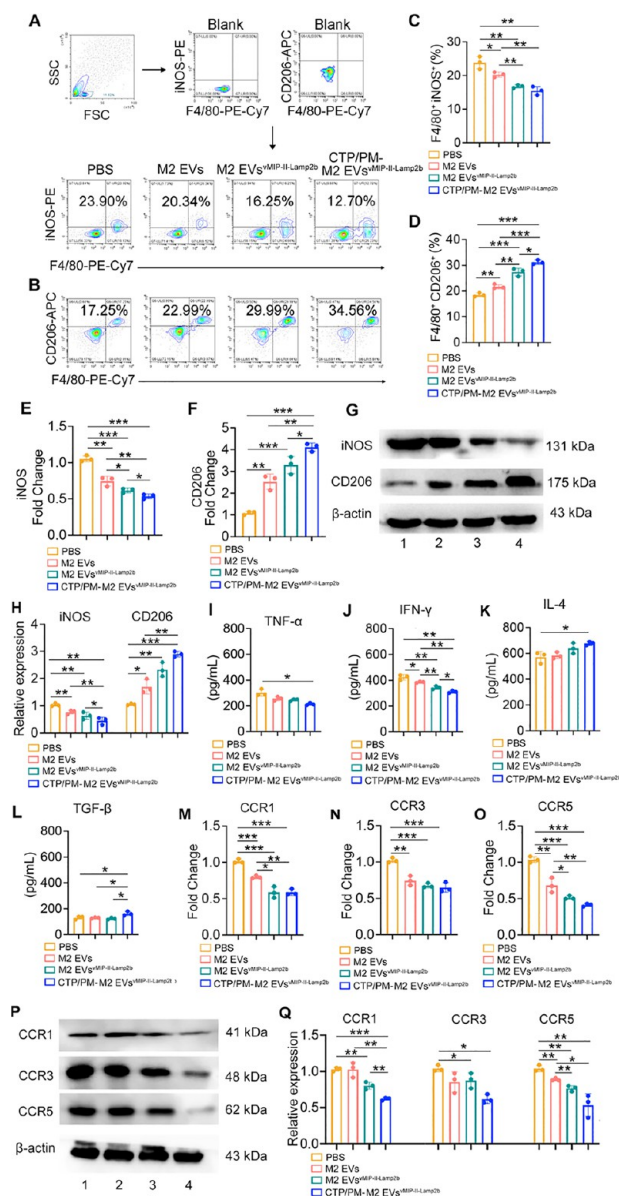


**Figure 10.** Immunoregulation of CTP/PM-M2 EVs<sup>vMIP-II-Lamp2b</sup> in vivo. (A) M1 macrophages (F4/80<sup>+</sup> iNOS<sup>+</sup>) were analyzed by flow cytometry 48 h after the last treatment ( $n = 5$  mice/per group). (B) M2 macrophages (F4/80<sup>+</sup> CD206<sup>+</sup>) macrophages were analyzed by flow cytometry 48 h after the last treatment ( $n = 5$  mice/per group). (C) A bar graph of M1 macrophage percentages in figure A. (D) A bar graph of M2 macrophage percentages in figure B. (E) Quantification of M1 macrophage (iNOS)- and (F) M2 macrophage (CD206)-related mRNA expression in the heart tissues 48 h after the last treatment ( $n = 5$  mice/per group). (G,H) Quantification of M1 macrophage (iNOS)- and M2 macrophage (CD206)-related protein expression in the heart tissues 48 h after the last treatment ( $n = 5$  mice/per group). 1, 2, 3, and 4 stand for PBS, M2 EVs, M2 EVs<sup>vMIP-II-Lamp2b</sup>, and CTP/PM-M2 EVs<sup>vMIP-II-Lamp2b</sup>. (I–L) Concentration of TNF- $\alpha$ , IFN- $\gamma$ , IL-4, and TGF- $\beta$  cytokines in hearts 48 h after last treatment ( $n = 3$  mice/per group). (M–O) Quantification of mRNA expression of CCR1, CCR3, and CCR5 in the heart tissues 48 h after the last treatment ( $n = 5$  mice/per group). (P,Q) Quantification of protein expression of CCR1, CCR3, and CCR5 in the heart tissues 48 h after the last treatment ( $n = 5$  mice/per group). 1, 2, 3, and 4 stand for PBS, M2 EVs, M2 EVs<sup>vMIP-II-Lamp2b</sup>, and CTP/PM-M2 EVs<sup>vMIP-II-Lamp2b</sup>. Results were presented as mean  $\pm$  SEM of three independent experiments. \* $P < 0.05$ ; \*\* $P < 0.01$ ; \*\*\* $P < 0.001$

Figure 10. continued

analyzed by one-way ANOVA followed by a multiple-comparison test.

and CCR5 compared with those of PBS treatment (Figure 10P,Q).

Previous studies have reported that abnormal differentiation of CD4<sup>+</sup> T cells (Th cells) plays an important role in the pathogenesis of VM, especially the increase in CD4<sup>+</sup> Th1 cells and the decrease in CD4<sup>+</sup> Th2 cells.<sup>29</sup> Therefore, we further examined whether EVs can regulate the proportion of the CD4<sup>+</sup> Th cell population in VM. Flow cytometry analysis showed that CTP/PM-M2 EVs<sup>vMIP-II-Lamp2b</sup> can play an immunoregulatory role in the hearts of VM mice compared with PBS, which is characterized by a decrease in the number of CD4<sup>+</sup> Th1 cells, accompanied by an increase in the number of CD4<sup>+</sup> Th2 cells (Figure S5B). In conclusion, CTP/PM-M2 EVs<sup>vMIP-II-Lamp2b</sup> can not only be internalized by cardiac macrophages but also reprogram macrophages into the M2 state, downregulate the expression level of chemokine receptors, and promote the resolution of the inflammatory immune microenvironment to help repair hearts.

**Therapeutic Efficacy of CTP/PM-M2 EVs<sup>vMIP-II-Lamp2b</sup> in Vivo.** To further demonstrate the cardiac repair role of CTP/PM-M2 EVs<sup>vMIP-II-Lamp2b</sup> in vivo, we evaluated cardiac remodeling and cardiac function in VM mice 48 h after the final administration. Compared with VM mice treated with PBS, the hearts of VM mice treated with CTP/PM-M2 EVs<sup>vMIP-II-Lamp2b</sup> showed a significant reduction in perivascular inflammatory cell infiltration (Figure 11A). Meanwhile, CTP/PM-M2 EVs<sup>vMIP-II-Lamp2b</sup> could reduce weight loss and serum cTnI levels in VM mice (Figure 11B,C). The ejection fraction (EF), fractional shortening (FS), LVEDD, and LVESD are important predictors of cardiac function. As shown in Figure 11D, the EF and FS of the CTP/PM-M2 EVs<sup>vMIP-II-Lamp2b</sup> treatment group were significantly increased compared to those of the PBS treatment group. Moreover, the LVESD and LVEDD of the CTP/PM-M2 EVs<sup>vMIP-II-Lamp2b</sup> group were significantly decreased compared to those of the PBS group. These results demonstrate that cardiac function improved after CTP/PM-M2 EVs<sup>vMIP-II-Lamp2b</sup> treatment.

**In Vivo Safety of CTP/PM-M2 EVs<sup>vMIP-II-Lamp2b</sup>.** During EVs treatment, the toxic side effects of EVs on normal organs and entire systems have represented major problems that warrant consideration. To confirm the biosafety of CTP/PM-M2 EVs<sup>vMIP-II-Lamp2b</sup> in vivo, major organs were first collected from VM mice 1 month after the last injection of PBS, M2 EVs, M2 EVs<sup>vMIP-II-Lamp2b</sup>, or CTP/PM-M2 EVs<sup>vMIP-II-Lamp2b</sup>. Compared with the PBS treatment group, no significant toxic changes were observed in H&E staining of major organs in the M2 EVs, M2 EVs<sup>vMIP-II-Lamp2b</sup>, or CTP/PM-M2 EVs<sup>vMIP-II-Lamp2b</sup> treatment groups within 1 month (Figure S6A). The peripheral blood of mice in each treatment group was also collected to determine multiple routine indices using an automatic blood cell analyzer. The results showed that after three treatments with M2 EVs, M2 EVs<sup>vMIP-II-Lamp2b</sup>, or CTP/PM-M2 EVs<sup>vMIP-II-Lamp2b</sup>, the number of white and red blood cells (WBC and RBC), hemoglobin content (HGB), platelet number (PLT), ratio or number of lymphocytes (LYM), monocytes (MO), and neutrophils (NEUT), and ratio or number of eosinophils (EO) and basophils (BA) in the peripheral blood of mice were not significantly different

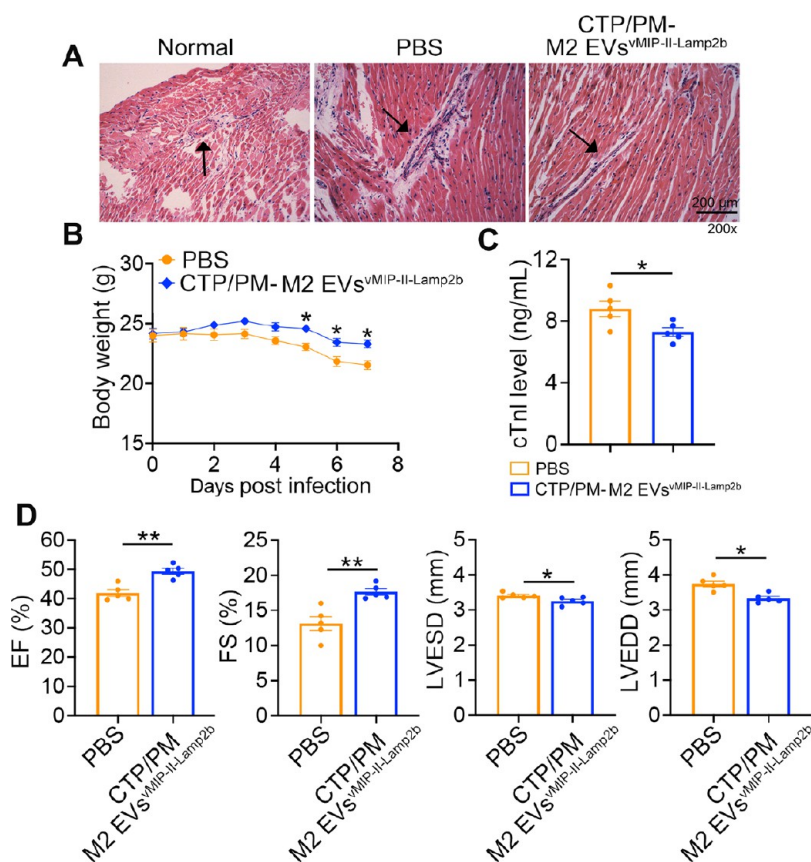


**Figure 11.** Therapeutic efficacy of CTP/PM-M2 EVs<sup>vMIP-II-Lamp2b</sup> in vivo. (A) Heart tissues were collected 48 h after the last treatment with PBS and CTP/PM-M2 EVs<sup>vMIP-II-Lamp2b</sup> and then stained with H&E ( $n = 5$  mice/per group). (B) The weight change of mice body ( $n = 5$  mice/per group). (C) The levels of cTnI in mice serum were determined by ELISA 48 h after the last treatment ( $n = 5$  mice/per group). (D) The EF, FS, LVEDD, and LVEDD measured based on the echocardiograms at week 4 (days 28) ( $n = 5$  mice/per group). Results were presented as mean  $\pm$  SEM and analyzed by a two-tailed Student's *t* test for single comparison. \* $P < 0.05$ ; \*\* $P < 0.01$ .

compared with those of the PBS treatment group. This indicates that neither M2 EVs, M2 EVs<sup>vMIP-II-Lamp2b</sup>, nor CTP/PM-M2 EVs<sup>vMIP-II-Lamp2b</sup> treatment significantly affected the peripheral blood routine indicators of VM mice (Figure S6B–D). Clinical biochemical analysis showed that the serum alanine aminotransferase (ALT), aspartate aminotransferase (AST), blood urea nitrogen (BUN), and creatinine (CRE) levels in mice were normal, indicating that the treatment did not affect the biological function of the liver and kidney (Figure S6E). To summarize, treatment with CTP/PM-M2 EVs<sup>vMIP-II-Lamp2b</sup> led to no significant immunotoxicity or side effects, indicating that they represent a safe candidate for the treatment of VM.

## CONCLUSION

In this study, we proposed a multitarget modified M2 EV-targeted immunomodulatory therapy for M1 macrophages for VM. M2 EVs with high vMIP-II expression, namely M2 EVs<sup>vMIP-II-Lamp2b</sup>, obtained by vMIP-II gene modification, not only help to increase the targeting ability of M2 EVs but also collaborate with M2 EVs to regulate M1 macrophages in the inflammatory microenvironment as well as downregulate the levels of CCR1, CCR3, and CCR5 in the heart tissues, which also helps to improve cardiac inflammation. Based on this, we developed the CTP-and-PM-engineered M2 EVs<sup>vMIP-II-Lamp2b</sup>, namely CTP/PM-M2 EVs<sup>vMIP-II-Lamp2b</sup>, to improve “cargo” delivery to the heart tissues. This multitarget modified M2 EVs

have been shown to efficiently target the heart tissues, combine with macrophages to exert immunomodulatory effects, and then reprogram M1 macrophages to M2, reduce the inflammatory response of the hearts, and promote the recovery of cardiac function. Finally, CTP/PM-M2 EVs<sup>vMIP-II-Lamp2b</sup> displayed a good safety profile without any significant side effects after three injections in VM mice. To sum up, our studies unveil the superior ability of CTP, PM, and vMIP-II to serve as targeting that helps deliver therapeutic M2 EVs to the injured lesions of VM.

## METHODS

**Mice.** BALB/c male mice (aged 6–8 weeks, 20–22 g) were purchased from GemPharmatechCo., Ltd. (Nanjing, China) and housed in pathogen-free mouse colonies. All animal experiments in the present study were performed according to the guidelines for the Care and Use of Laboratory Animals (Ministry of Health, China, 1998) and the guidelines of the Laboratory Animal Ethical Commission of Wannan Medical College. All experimental protocols were evaluated and approved by the Animal Ethical Committee of Wannan Medical College (approval number: LLSC-2022-198).

**Cell Culture.** J774A.1 and THP-1 cells were purchased from Servicebio (Guangzhou, China). J774A.1 cells were cultured in DMEM complete medium supplemented with fetal bovine serum (FBS; 10% v/v, 10100147, Gibco) and penicillin-streptomycin. M1 macrophages were stimulated with 100 ng/mL lipopolysaccharide (LPS) and 20 ng/mL IFN- $\gamma$  for 24 h, and M2 macrophages were induced with 20 ng/mL IL-4 and IL-13 for 48 h. THP-1 cells were cultured in RPMI 1640 medium with 20% FBS and 1% penicillin-

streptomycin. Then, cells were treated with 200 ng/mL phorbol-12-myristate-13-acetate (PMA) for 48 h, followed by further 48 h incubation with IFN- $\gamma$  (20 ng/mL) and LPS (100 ng/mL) to polarize the cells toward M1. All cells were cultured at 37 °C with 5% CO<sub>2</sub>.

**Transfection of Lentivirus.** J774A.1 cells were seeded in 24-well plates and incubated at 37 °C in 5% CO<sub>2</sub>. After reaching approximately 50% confluence, the cells were cotransfected with vMIP-II-Lamp2b-GFP lentivirus or mock-Lamp2b-GFP lentivirus (Sangon Biotech, Shanghai, China) according to the manufacturer's instructions. J774A.1 cells were infected with lentiviruses in the presence of 6–8  $\mu$ g/mL Polybrene (Sigma-Aldrich), and those that stably expressed vMIP-II were enriched by puromycin selection for positive clones. Next, cytokines IL-4 and IL-13 were added to stimulate and induce M2 macrophages.

**Preparation of M2 EVs and M2 EVs<sup>vMIP-II-Lamp2b</sup>.** M2 EVs and M2 EVs<sup>vMIP-II-Lamp2b</sup> were prepared from the supernatant of mock-Lamp2b-M2 macrophages or vMIP-II-M2 macrophages by SEC (size exclusion chromatography) methods (Exosupur Kit, Echobiotech, China) or using differential centrifugation. M0 EVs were also prepared from J774A.1 cells without stimulation or lentiviral transfection. Briefly, the supernatant was centrifuged at 300g for 10 min, 3000g for 15 min, and 10 000g for 60 min at 4 °C to remove cells and debris, before filtering using a 0.22  $\mu$ m filter (Millipore, USA). The filtrate was centrifuged at 110 000g for 2 h at 4 °C using an XPN-100 ultracentrifuge (Beckman Coulter, USA). Subsequently, the pellet was resuspended in phosphate-buffered saline (PBS) and then ultracentrifuged again at 110 000g for 2 h. Finally, the resulting pellet was resuspended in PBS for further study.

**Preparation of CTP-M2 EVs.** A phospholipid-based membrane anchor, 1,2-dioleoyl-*sn*-glycero-3-phosphoethanolamine-N-(polyethylene glycol)-succinyl-N hydroxysuccinimidyl ester (DOPE-PEG-NHS), was purchased from Ruixi Biological Technology (Xi'an, China). The M.W. of poly(ethylene glycol) (PEG) was 2000 Da. Briefly, 20  $\mu$ g of streptomycin (SA) was incubated with 300  $\mu$ g of DOPE-PEG-NHS solution in dimethyl sulfoxide at 37 °C for 4 h, and the SA was coupled to the NHS end. Next, peptides (30  $\mu$ g) of biotinylated CTP were added, and the mixture was incubated for another 24 h. The reaction was terminated with Tris-HCl buffer (1 M, pH 8.0). Finally, M2 EVs (200  $\mu$ g) were added to the above mixture and incubated at 37 °C for 4 h to obtain CTP-M2 EVs.

**Isolation of Platelets (PLT).** Fresh whole blood samples were taken from healthy mice, and PLTs were isolated through gradient centrifugation. Briefly, 0.5 mL of whole blood (from five mice) was centrifuged at 200g for 10 min, and the supernatant was isolated as platelet-rich plasma (PRP). Next, PRP was centrifuged at 1800g for 20 min before removing the supernatant and precipitating it into platelets. Platelets were obtained by washing the precipitate with PBS three times and then resuspending in PBS containing 1 mM EDTA and 2  $\mu$ M prostaglandin E1 (PGE1).

**Fabrication of PM.** The PLT suspension was frozen at –80 °C for 10 min and thawed to room temperature for 5 min; this process was repeated three times. Subsequently, the suspension was centrifuged at 8000g for 10 min to isolate the PM, which was then sonicated for 5 min at a frequency of 40 kHz and 100 W using a bath sonicator, resulting in a PM fragment suspension. Finally, the PM was extracted through a 400 nm polyester porous membrane.

**Preparation of PM-M2 EVs and CTP/PM-M2 EVs<sup>vMIP-II-Lamp2b</sup>.** Next, PM-coated M2 EVs (PM-M2 EVs) or M2 EVs<sup>vMIP-II-Lamp2b</sup> were obtained by coextruding the PM and M2 EVs or M2 EVs<sup>vMIP-II-Lamp2b</sup> through a 200 nm polyester porous membrane for at least 10–20 passes. For preparation of CTP/PM-M2 EVs<sup>vMIP-II-Lamp2b</sup>, briefly, 20  $\mu$ g of SA was incubated with 300  $\mu$ g of DOPE-PEG-NHS solution in dimethyl sulfoxide at 37 °C for 4 h, and the SA was coupled to the NHS end. Next, peptides (30  $\mu$ g) of biotinylated CTP were added and incubated for another 24 h. The reaction was terminated with Tris-HCl buffer (1 M, pH 8.0). Finally, PM-coated M2 EVs<sup>vMIP-II-Lamp2b</sup> (200  $\mu$ g) were added to the above mixture and incubated at 37 °C for 4 h to obtain CTP/PM-M2 EVs<sup>vMIP-II-Lamp2b</sup>.

**Characterization of EVs.** M2 EVs, M2 EVs<sup>vMIP-II-Lamp2b</sup>, PM-M2 EVs, CTP-M2 EVs, and CTP/PM-M2 EVs<sup>vMIP-II-Lamp2b</sup> were

precipitated on a carbon-coated grid and stained with 1% phosphotungstic acid for transmission electron microscopy (TEM) observation. The particle concentration and size were determined through nanoparticle tracking analysis (NTA) via ZetaView PMX. The surface zeta potential was measured with dynamic light scattering using a Zetasizer Nano ZS90 (Malvern Instruments, UK). Additionally, purified EVs were verified by Western blotting analysis using the following antibodies: anti-vMIP-II (1:1000, 601-VB, R&D Systems), anti-CD63 (1:1000, ab271286, Abcam), anti-HSP70 (1:500, ab2787, Abcam), anti-calnexin (1:1000, ab133615, Abcam). Briefly, 2–5 mg EVs were homogenized in a lysis buffer (S3401, Sigma) containing protease and phosphatase inhibitors (P1045, Beyotime). EV lysates containing 50  $\mu$ g of proteins in SDS sample buffer were subjected to electrophoresis using polyacrylamide gels and transferred onto PVDF membranes. The membranes were blocked and then incubated with horseradish-peroxidase-conjugated secondary antibody for 1 h. Finally, the signals were detected using an Automatic Chemiluminescence Image Analysis System (Tanon 5200, Tanon Science & Technology). For the serum stability test, CTP/PM-M2 EVs<sup>vMIP-II-Lamp2b</sup> were resuspended in serum and incubated for 48 h to observe the changes in particle size and number.

To verify the successful loading of CTP and PM onto the CTP/PM-M2 EVs<sup>vMIP-II-Lamp2b</sup> surface, CTP labeled with AMCA [7-amino-4-methylcoumarin] and PM labeled with PKH26 (Umbio (Shanghai) Co., Ltd.) were loaded onto the EVs' surface to observe colocalization using a confocal laser scanning microscope (CLSM). The exact ratio of PM and CTP successfully loaded onto the EVs surface was measured by using flow cytometry.

**Cytotoxicity Assessment of EVs.** To evaluate the cytotoxicity of several types of EVs in vitro, BMDMs (approximately  $3 \times 10^5$  cells) were seeded with 200  $\mu$ g/mL M2 EVs, M2 EVs<sup>vMIP-II-Lamp2b</sup>, PM-M2 EVs, CTP-M2 EVs, or CTP/PM-M2 EVs<sup>vMIP-II-Lamp2b</sup> in triplicate in a 24-well plate (NEST Biotechnology). After 4 h of incubation, cells were collected for apoptosis detection by flow cytometry.

**Internalization of EVs in Vitro.** THP-1 cells and BMDMs were stimulated to M1 macrophages according to the previously described method<sup>37</sup> and then treated with PKH26-labeled M2 EVs, M2 EVs<sup>vMIP-II-Lamp2b</sup>, PM-M2 EVs, CTP-M2 EVs, or CTP/PM-M2 EVs<sup>vMIP-II-Lamp2b</sup> for different times (0.5, 1, 4, and 24 h) to explore internalization efficiency. Finally, we observed the internalization efficiency of EVs under CLSM or by using flow cytometry. To further detect the mechanism of internalization of EVs, BMDMs were stimulated to M1 macrophages and then pretreated with different inhibitors (80  $\mu$ M Dynasore, 20  $\mu$ M nystatin, 10  $\mu$ M chlorpromazine, and 100  $\mu$ M amiloride) for 30 min respectively, followed by the addition of PKH26-labeled M2 EVs, M2 EVs<sup>vMIP-II-Lamp2b</sup>, PM-M2 EVs, CTP-M2 EVs, or CTP/PM-M2 EVs<sup>vMIP-II-Lamp2b</sup> for 1 h.

**Endosome Escape Ability of EVs.** M1 macrophages (BMDMs) were treated with PKH26-labeled M2 EVs, M2 EVs<sup>vMIP-II-Lamp2b</sup>, PM-M2 EVs, CTP-M2 EVs, or CTP/PM-M2 EVs<sup>vMIP-II-Lamp2b</sup> (50  $\mu$ g EVs/ $10^6$  cells) for different times (1, 6, and 24 h) to explore the endosome escape ability. Briefly, after cells were treated with EVs, the cell culture medium was removed, a 37 °C preincubated LysoTracker-green solution (Beyotime) was added, and the cells were incubated for 10 min. Finally, the cells were rinsed and stained with DAPI for another 10 min, which were observed under CLSM.

**Immunomodulatory Effects of CTP/PM-M2 EVs<sup>vMIP-II-Lamp2b</sup> in Vitro.** To detect the ability of CTP/PM-M2 EVs<sup>vMIP-II-Lamp2b</sup> to reprogram macrophages from the M1 to M2, M2 EVs, M2 EVs<sup>vMIP-II-Lamp2b</sup>, PM-M2 EVs, CTP-M2 EVs, or CTP/PM-M2 EVs<sup>vMIP-II-Lamp2b</sup> were incubated with M1 macrophages (BMDMs) for 48 h, before the cells were collected for RNA extraction, Western blotting, and flow cytometry. For flow cytometry analysis, the cells (approximately  $5 \times 10^5$  cells) were stained with 1  $\mu$ g of PE-Cy7-conjugated anti-F4/80 antibody (BM8, Thermo Fisher Scientific) and APC-conjugated anti-CD206 antibody (MR6F3, Thermo Fisher Scientific) or PE-conjugated anti-iNOS antibody (CXNFT, Thermo Fisher Scientific).

Quantitative reverse transcription-polymerase chain reaction (qRT-PCR) were used to detect the changes in chemokine receptors and M1 and M2 macrophage markers; this protocol refers to our previous study.<sup>38</sup> The primers are shown in Table S1. Additionally, chemokine receptors and M1 and M2 macrophage markers were verified by Western blot analysis using the following antibodies: anti-iNOS (1:1000, ab178945, Abcam), anti-CD206 (1:1000, ab300621, Abcam), anti-CCR1 (1:1000, MAB5986, R&D Systems), anti-CCR3 (1:1000, orb1595875, Biorbyt), and anti-CCR5 (1:1000, MAB6138, R&D Systems). For details about the procedure, see Part 2.9.

**Virus and Myocarditis Model.** The original stock of CVB3 (Nancy strain) was a gift from Professor Wei Hou (School of Basic Medical Sciences, Wuhan University) and was maintained by passage through HeLa cells (ATCC number: CCL-2). The viral titer was routinely determined before infection using a 50% tissue culture infectious dose (TCID<sub>50</sub>) assay of HeLa cell monolayers. Mice were infected by intraperitoneal injection of 0.2 mL of PBS containing approximately  $1 \times 10^5$  plaque-forming units (PFU) of the virus.

**Preparation of Cardiac Single-Cell Suspension.** Mouse hearts were first collected and transferred to a 10 cm Petri dish containing PBS, and each heart was cut into small pieces. The harvested tissues were transferred into a gentleMACS C tube and incubated at 37 °C for 15 min with a 5 mL enzyme mixture (2 mg/mL Collagenase IV and 0.5 mg/mL Dispase II). Then, the C tube was attached onto the sleeve of the gentle MACS Dissociator, and the gentleMACS Program *m\_heart\_01* was run for a total of three times to obtain the cell suspension. Next, a cell suspension was centrifuged at 600g for 5 min, and a cell pellet was resuspended in 1× Red Blood Cell Lysis Solution to remove RBCs. At last, cells were centrifuged at 600g for 5 min two times and resuspended in PBS for further applications.

**Biodistribution of DiD-Labeled CTP/PM-M2 EVs<sup>vMIP-II-Lamp2b</sup> in Vivo.** Having determined the function of CTP/PM-M2 EVs<sup>vMIP-II-Lamp2b</sup> in vitro, we next evaluated the pharmacokinetics of these EVs in vivo. To this end, DiD-labeled M2 EVs, M2 EVs<sup>vMIP-II-Lamp2b</sup>, PM-M2 EVs, CTP-M2 EVs, and CTP/PM-M2 EVs<sup>vMIP-II-Lamp2b</sup> at a dosage of 200 μg were injected into mice via the tail vein on day 3. Then, the fluorescence intensity was observed in vivo using an Imaging System (AniView600, Guangzhou Biolight Biotechnology Co., Ltd.).

**Targeting Ability of CTP/PM-M2 EVs<sup>vMIP-II-Lamp2b</sup> in Vivo.** To study the in vivo targeting ability of EVs, a myocarditis model was established as above, administered with DiD (red)-labeled M2 EVs, M2 EVs<sup>vMIP-II-Lamp2b</sup>, PM-M2 EVs, CTP-M2 EVs, and CTP/PM-M2 EVs<sup>vMIP-II-Lamp2b</sup> on day 3 and sacrificed 24 h postadministration. Heart tissues were harvested and prepared as a single-cell suspension. The proportion of DiD-labeled M2 EVs, M2 EVs<sup>vMIP-II-Lamp2b</sup>, PM-M2 EVs, CTP-M2 EVs, and CTP/PM-M2 EVs<sup>vMIP-II-Lamp2b</sup> in the heart macrophages and Ly6C monocytes was analyzed by flow cytometry.

**Immunomodulatory Effects of CTP/PM-M2 EVs<sup>vMIP-II-Lamp2b</sup> in Vivo.** VM mice were injected with M2 EVs, M2 EVs<sup>vMIP-II-Lamp2b</sup>, or CTP/PM-M2 EVs<sup>vMIP-II-Lamp2b</sup> through the tail vein on days 1, 3, and 5, respectively, and euthanized 48 h after the last administration to observe their anti-inflammatory effects. The hearts were digested to obtain a single-cell suspension, which was incubated with PE-Cy7-anti F4/80 (BM8, Thermo Fisher Scientific), PE-anti iNOS (CXNFT, Thermo Fisher Scientific), APC-anti CD206 (MR6F3, Thermo Fisher Scientific), PE-anti IFN-γ (4S.B3, Thermo Fisher Scientific), PE-anti IL-4 (11B11, Thermo Fisher Scientific), or FITC-anti CD4 antibodies (RPA-T4, Thermo Fisher Scientific). For intracellular staining, cells were fixed and permeabilized using fixation buffer and permeabilization solution (Thermo Fisher Scientific), respectively. The levels of iNOS, CD206, CCR1, CCR3, and CCR5 were measured by qRT-PCR and Western blotting. Additionally, the homogenized hearts of mice following the last treatment were collected to detect the concentrations of proinflammatory cytokines (IFN-γ, TNF-α) and anti-inflammatory cytokines (IL-4, TGF-β) using ELISA (R&D Systems).

**Nitric Oxide (NO) Production Assay.** The tissue homogenate infiltrated by cardiac macrophages of VM mice was first prepared, and

then, 50 μL aliquots of the tissue homogenate were mixed with 50 μL of Griess reagent (Beyotime Biotechnology, China) and incubated for 10 min at room temperature. The colorimetric reaction was then measured at 540 nm by using a Multiskan Go microplate reader (Thermo Scientific).

**Cardiac Histopathology.** The mice in each treatment group were injected with precooled PBS and paraformaldehyde successively through the heart under deep anesthesia. Subsequently, the hearts were removed and soaked in fresh 4% neutral buffered paraformaldehyde at room temperature for 24 h. The paraffin-embedded tissues were sliced (7 μm thickness), followed by hematoxylin and eosin (H&E) staining.

**Cardiac Dysfunction Measurement.** Cardiac dysfunction was measured by blinded echocardiography analysis using a FUJIFILM Evo 3100 LT Ultrasound System on days 28. Each measurement was performed for at least three consecutive cardiac cycles. At the papillary muscle level, the left ventricular end-systolic diameter (LVESD) and LV end-diastolic diameter (LVEDD) were measured by long-axis views of M-mode tracings. The LV ejection fraction (EF) and fractional shortening (FS) were calculated based on the LVESD and LVEDD.

**In Vivo Safety Assessment.** VM mice were intravenously injected with M2 EVs<sup>vMIP-II-Lamp2b</sup> or CTP/PM-M2 EVs<sup>vMIP-II-Lamp2b</sup> on days 1, 3, and 5. On days 28, the mice were sacrificed, and the major organs (liver, spleen, lung, and kidney) were obtained for H&E staining. Additionally, the blood of mice in all groups was collected and immediately analyzed for hematological parameters.

**Statistics.** Statistical analysis was performed by using GraphPad Prism 9.1.1 software. For comparison of two groups, *P* values were determined by an unpaired two-tailed Student's *t* test, and the multiple-group data were compared by one-way ANOVA followed by a multiple-comparison test. A *P* value of less than 0.05 was considered significant.

## ASSOCIATED CONTENT

### Supporting Information

The Supporting Information is available free of charge at <https://pubs.acs.org/doi/10.1021/acsnano.3c05847>.

Supplementary Table, namely Primers used for qPCR. Supplementary figures, namely Identification of M2 EVs<sup>vMIP-II-Lamp2b</sup>; Characterization of EVs; Cargo transport of CTP/PM-M2 EVs<sup>vMIP-II-Lamp2b</sup> in vitro; DiD-labeled EVs in spleens, lungs, kidneys, livers, and guts of VM mice; Immunoregulation of CTP/PM-M2 EVs<sup>vMIP-II-Lamp2b</sup> in vivo; Biosafety of EVs in vivo (PDF)

## AUTHOR INFORMATION

### Corresponding Authors

**Kun Lv** – Central Laboratory, The first affiliated hospital of Wannan Medical College, Wuhu 241000, P.R. China; Anhui Province Key Laboratory of Non-coding RNA Basic and Clinical Transformation, Wuhu 241000, P.R. China; Anhui Province Clinical Research Center for Critical Respiratory Medicine, Wuhu 241000, P.R. China; [orcid.org/0000-0002-1895-6700](https://orcid.org/0000-0002-1895-6700); Phone: +86-553-5739912; Email: [lvkun315@126.com](mailto:lvkun315@126.com); Fax: +86-553-5739209

**Hezuo Lü** – Department of Clinical Laboratory, The First Affiliated Hospital of Bengbu Medical University, Bengbu 233030, P.R. China; Anhui Key Laboratory of Tissue Transplantation, Bengbu Medical University, Bengbu 233030, P.R. China; Email: [lh233003@163.com](mailto:lh233003@163.com)

### Authors

**Weiya Pei** – Central Laboratory, The first affiliated hospital of Wannan Medical College, Wuhu 241000, P.R. China; Anhui

Province Key Laboratory of Non-coding RNA Basic and Clinical Transformation, Wuhu 241000, P.R. China; Anhui Province Clinical Research Center for Critical Respiratory Medicine, Wuhu 241000, P.R. China

**Yingying Zhang** – Department of Laboratory Medicine, The First Affiliated Hospital of Wannan Medical College, Wuhu 241000, P.R. China

**Xiaolong Zhu** – Central Laboratory, The first affiliated hospital of Wannan Medical College, Wuhu 241000, P.R. China; Anhui Province Key Laboratory of Non-coding RNA Basic and Clinical Transformation, Wuhu 241000, P.R. China; Anhui Province Clinical Research Center for Critical Respiratory Medicine, Wuhu 241000, P.R. China

**Chen Zhao** – Suzhou Hospital, Affiliated Hospital of Medical School, Nanjing University, Suzhou 215163, P.R. China

**Xueqin Li** – Central Laboratory, The first affiliated hospital of Wannan Medical College, Wuhu 241000, P.R. China; Anhui Province Key Laboratory of Non-coding RNA Basic and Clinical Transformation, Wuhu 241000, P.R. China; Anhui Province Clinical Research Center for Critical Respiratory Medicine, Wuhu 241000, P.R. China

Complete contact information is available at:  
<https://pubs.acs.org/10.1021/acsnano.3c05847>

#### Author Contributions

Pei, W. Y., Zhang, Y. Y., and Zhu, X. L. contributed equally to this work. Lv, K. and Lü, H. Z. designed the research project. Pei, W. Y. and Zhu, X. L. performed the experiments, analyzed data, and wrote the manuscript. Zhao, C. helped to perform the biological experiments. Li, X. Q. helped to analyze data. All authors have consented to the final version of the manuscript.

#### Notes

The authors declare no competing financial interest.

#### ACKNOWLEDGMENTS

This work was supported by the National Natural Science Foundation of China (82100019, 82170368, 82072370, 81772180, 81870017, 81701557, 81802503), Natural Science Foundation of Anhui Province (2108085QH307, 2108085J44), Program for Excellent Sci-tech Innovation Teams of Universities in Anhui Province (2022AH010074), Innovation fund for Industry-University-Research of Chinese universities (2023HT008), Wuhu Science and Technology Project (2022jc56), Funding of “Peak” Training Program for Scientific Research of Yijishan Hospital, Wannan Medical College (GF2019T01 and GF2019G09). We thank LetPub ([www.letpub.com](http://www.letpub.com)) for its linguistic assistance during the preparation of this manuscript.

#### ABBREVIATIONS

APC: allophycocyanin  
Arg-1: arginase 1  
BALF: bronchoalveolar lavage fluid  
BFA: brefeldin A  
BMDM: bone-marrow-derived macrophage  
CLSM: confocal laser scanning microscope  
CTP: cardiac-targeting peptide  
CVB3: coxsackievirus B3  
EVs: extracellular vesicles  
FITC: fluorescein isothiocyanate  
IFN: interferon  
LPS: lipopolysaccharide

M1: classically activated macrophages  
M2: alternatively activated macrophages  
PE: phycoerythrin  
PE-Cy7: phycoerythrin-Cy7  
PFA: paraformaldehyde  
PMA: phorbol 12-myristate 13-acetate  
PM: platelet membranes  
vMIP-II: viral macrophage inflammatory protein-II

#### REFERENCES

- Zheng, Q.; Zhuang, Z.; Wang, Z. H.; Deng, L. H.; Jin, W. J.; Huang, Z. J.; Zheng, G. Q.; Wang, Y. Clinical and Preclinical Systematic Review of Astragalus Membranaceus for Viral Myocarditis. *Oxid Med. Cell Longev* **2020**, *2020*, 1560353.
- Sagar, S.; Liu, P. P.; Cooper, L. T., Jr Myocarditis. *Lancet* **2012**, *379*, 738–47.
- Rivadeneira, L.; Charó, N.; Kviatcovsky, D.; de la Barrera, S.; Gómez, R. M.; Schattner, M. Role of neutrophils in CVB3 infection and viral myocarditis. *J. Mol. Cell Cardiol* **2018**, *125*, 149–161.
- Hou, X. Z.; Chen, G. B.; Bracamonte-Baran, W.; Choi, H. S.; Diny, N. L.; Sung, J.; Hughes, D.; Won, A.; Wood, M. K.; et al. The Cardiac Microenvironment Instructs Divergent Monocyte Fates and Functions in Myocarditis. *Cell Rep* **2019**, *28*, 172–189.e7.
- Fairweather, D.; Rose, N. R. Coxsackievirus-induced myocarditis in mice: a model of autoimmune disease for studying immunotoxicity. *Methods* **2007**, *41*, 118–122.
- Hua, X. M.; Hu, G.; Hu, Q. T.; Chang, Y.; Hu, Y. T.; Gao, L. L.; Chen, X.; Yang, P. C.; Zhang, Y.; Li, M. Y.; Song, J. P. Single-Cell RNA Sequencing to Dissect the Immunological Network of Autoimmune Myocarditis. *Circulation* **2020**, *142*, 384–400.
- Zhang, Y. Y.; Li, X. Q.; Kong, X.; Zhang, M. Y.; Wang, D. G.; Liu, Y. H.; Lv, K. Long non-coding RNA AK085865 ablation confers susceptibility to viral myocarditis by regulating macrophage polarization. *J. Cell Mol. Med.* **2020**, *24*, 5542–5554.
- Xue, Y. L.; Zhang, S. X.; Zheng, C. F.; Li, Y. F.; Zhang, L. H.; Su, Q. Y.; Hao, Y. F.; Wang, S.; Li, X. W. Long non-coding RNA MEG3 inhibits M2 macrophage polarization by activating TRAF6 via microRNA-223 down-regulation in viral myocarditis. *J. Cell Mol. Med.* **2020**, *24*, 12341–12354.
- Zhang, Y.; Cai, S. B.; Ding, X. X.; Lu, C.; Wu, R. D.; Wu, H. Y.; Shang, Y. Y.; Pang, M. J. MicroRNA-30a-5p silencing polarizes macrophages toward M2 phenotype to alleviate cardiac injury following viral myocarditis by targeting SOCS1. *Am. J. Physiol Heart Circ Physiol* **2021**, *320*, H1348–H1360.
- He, C. J.; Zheng, S.; Luo, Y.; Wang, B. Exosome Theranostics: Biology and Translational Medicine. *Theranostics* **2018**, *8*, 237–255.
- Zhao, R. J.; Wang, L.; Wang, T.; Xian, P. P.; Wang, H. K.; Long, Q. F. Inhalation of MSC-EVs is a noninvasive strategy for ameliorating acute lung injury. *J. Controlled Release* **2022**, *345*, 214–230.
- Hu, Q.; Lyon, C. J.; Fletcher, J. K.; Tang, W.; Wan, M.; Hu, T. Y. Extracellular vesicle activities regulating macrophage- and tissue-mediated injury and repair responses. *Acta Pharm. Sin B* **2021**, *11*, 1493–1512.
- Tang, T. T.; Wang, B.; Wu, M.; Li, Z. L.; Feng, Y.; Cao, J. Y.; Yin, D.; Liu, H.; Tang, R. N.; Crowley, S. D.; Lv, L. L.; Liu, B. C. Extracellular vesicle-encapsulated IL-10 as novel nanotherapeutics against ischemic AKI. *Sci. Adv.* **2020**, *6*, eaaz0748.
- Wang, C.; Dong, C. S.; Xiong, S. D. IL-33 enhances macrophage M2 polarization and protects mice from CVB3-induced viral myocarditis. *J. Mol. Cell Cardiol* **2017**, *103*, 22–30.
- Sesti-Costa, R.; Silva, G. K.; Proença-Módena, J. L.; Carlos, D.; Silva, M. L.; Alves-Filho, J. C.; Arruda, E.; Liew, F. Y.; Silva, J. S. The IL-33/ST2 pathway controls coxsackievirus B5-induced experimental pancreatitis. *J. Immunol* **2013**, *191*, 283–292.
- Yang, H. H.; Chen, Y.; Gao, C. Y. Interleukin-13 reduces cardiac injury and prevents heart dysfunction in viral myocarditis via

enhanced M2 macrophage polarization. *Oncotarget* **2017**, *8*, 99495–99503.

(17) Nguyen, V. V.T.; Witwer, K. W.; Verhaar, M. C.; Strunk, D.; van Balkom, B. W. M. Functional assays to assess the therapeutic potential of extracellular vesicles. *J. Extracell Vesicles* **2020**, *10*, e12033.

(18) Maas, S. L. N.; Breakefield, X. O.; Weaver, A. M. Extracellular Vesicles: Unique Intercellular Delivery Vehicles. *Trends Cell Biol.* **2017**, *27*, 172–188.

(19) Balbi, C.; Vassalli, G. Exosomes: Beyond stem cells for cardiac protection and repair. *Stem Cell* **2020**, *38*, 1387–1399.

(20) Françoço, M. C. S.; Costa, F. R. C.; Guerra-Gomes, I. C.; Silva, J.; Sesti-Costa, R. Dendritic cells and regulatory T cells expressing CCR4 provide resistance to coxsackievirus B5-induced pancreatitis. *Sci. Rep* **2019**, *9*, 14766.

(21) Valaperti, A.; Nishii, M.; Liu, Y.; Naito, K.; Chan, M.; Zhang, L.; Skurk, C.; Schultheiss, H. P.; Wells, G. A.; Eriksson, U.; Liu, P. P. Innate immune interleukin-1 receptor-associated kinase 4 exacerbates viral myocarditis by reducing CCR5(+) CD11b(+) monocyte migration and impairing interferon production. *Circulation* **2013**, *128*, 1542–54.

(22) Müller, I.; Pappritz, K.; Savvatis, K.; Puhl, K.; Dong, F.; El-Shafee, M.; Hamdani, N.; Hamann, I.; Noutsias, M.; Infante-Duarte, C.; Linke, W. A.; Van Linthout, S.; Tschöpe, C. CX3CR1 knockout aggravates Coxsackievirus B3-induced myocarditis. *PLoS One* **2017**, *12*, No. e0182643.

(23) Nguyen, A. F.; Kuo, N. W.; Showalter, L. J.; Ramos, R.; Dupureur, C. M.; Colvin, M. E.; LiWang, P. J. Biophysical and Computational Studies of the vCCI:vMIP-II Complex. *Int. J. Mol. Sci.* **2017**, *18*, 1778.

(24) Baba, O.; Huang, L. H.; Elvington, A.; Szpakowska, M.; Sultan, D.; Heo, G. S.; Zhang, X. H.; Luehmann, H.; Detering, L.; Chevigne, A.; Liu, Y. J.; Randolph, G. J. CXCR4-Binding Positron Emission Tomography Tracers Link Monocyte Recruitment and Endothelial Injury in Murine Atherosclerosis. *Arterioscler Thromb Vasc Biol.* **2021**, *41*, 822–836.

(25) Li, Q. Y.; Huang, Z. Y.; Wang, Q. Z.; Gao, J. F.; Chen, J.; Tan, H. P.; Li, S.; Wang, Z. M.; Weng, X. Y.; Yang, H. B.; Pang, Z. Q.; Song, Y. N.; Qian, J. Y.; Ge, J. B. Targeted immunomodulation therapy for cardiac repair by platelet membrane engineering extracellular vesicles via hitching peripheral monocytes. *Biomaterials* **2022**, *284*, 121529.

(26) Li, Q. Y.; Song, Y. N.; Wang, Q. Z.; Chen, J.; Gao, J. F.; Tan, H. P.; Li, S.; Wu, Y.; Yang, H. B.; Huang, H. W.; Yu, Y.; Li, Y.; Zhang, N.; Huang, Z. Y.; Pang, Z. Q.; Qian, J. Y.; Ge, J. B. Engineering extracellular vesicles with platelet membranes fusion enhanced targeted therapeutic angiogenesis in a mouse model of myocardial ischemia reperfusion. *Theranostics* **2021**, *11*, 3916–3931.

(27) Hu, S. Q.; Wang, X. Y.; Li, Z. H.; Zhu, D. S.; Cores, J.; Wang, Z. Z.; Li, J. L.; Mei, X.; Cheng, X.; Su, T.; Cheng, K. Platelet membrane and stem cell exosome hybrid enhances cellular uptake and targeting to heart injury. *Nano Today* **2021**, *39*, 101210.

(28) Imakawa, K.; Matsuno, Y.; Fujiwara, H. New Roles for EVs, miRNA and lncRNA in Bovine Embryo Implantation. *Front Vet Sci.* **2022**, *9*, 944370.

(29) Yue-Chun, L.; Gu, X. H.; Li-Sha, G.; Zhou, D. P.; Xing, C.; Guo, X. L.; Pan, L. L.; Song, S. Y.; Yu, L. L.; Chen, G. Y.; Lin, J. F.; Chu, M. P. Vagus nerve plays a pivotal role in CD4+ T cell differentiation during CVB3-induced murine acute myocarditis. *Virulence* **2021**, *12*, 360–376.

(30) Wang, Y.; Li, C. F.; Zhao, R. Z.; Qiu, Z. M.; Shen, C. Y.; Wang, Z. L.; Liu, W. W.; Zhang, W.; Ge, J. B.; Shi, B. CircUbe3a from M2 macrophage-derived small extracellular vesicles mediates myocardial fibrosis after acute myocardial infarction. *Theranostics* **2021**, *11*, 6315–6333.

(31) Zheng, P. M.; Chen, L.; Yuan, X. L.; Luo, Q.; Liu, Y.; Xie, G. H.; Ma, Y. H.; Shen, L. S. Exosomal transfer of tumor-associated macrophage-derived miR-21 confers cisplatin resistance in gastric cancer cells. *J. Exp Clin Cancer Res.* **2017**, *36*, 53.

(32) Lin, F.; Yin, H. B.; Li, X. Y.; Zhu, G. M.; He, W. Y.; Gou, X. Bladder cancer cell-secreted exosomal miR-21 activates the PI3K/AKT pathway in macrophages to promote cancer progression. *Int. J. Oncol.* **2020**, *56*, 151–164.

(33) Chen, Y.; Lin, J. H.; Schlotterer, A.; Kurowski, L.; Hoffmann, S.; Hammad, S.; Dooley, S.; Buchholz, M.; Hu, J.; Fleming, I.; Hammes, H. P. MicroRNA-124 Alleviates Retinal Vasoregression via Regulating Microglial Polarization. *Int. J. Mol. Sci.* **2021**, *22*, 11068.

(34) Yang, Y. X.; Ye, Y. Q.; Fan, K. X.; Luo, J. N.; Yang, Y. J.; Ma, Y. MiR-124 Reduced Neuroinflammation after Traumatic Brain Injury by Inhibiting TRAF6. *Neuroimmunomodulation* **2023**, *30*, 55–68.

(35) Yin, J.; Zhao, X. S.; Chen, X. J.; Shen, G. X. Emodin suppresses hepatocellular carcinoma growth by regulating macrophage polarization via microRNA-26a/transforming growth factor beta 1/protein kinase B. *Bioengineered* **2022**, *13*, 9549–9564.

(36) Odaka, C.; Mizuochi, T. Role of macrophage lysosomal enzymes in the degradation of nucleosomes of apoptotic cells. *J. Immunol* **1999**, *163*, 5346–52.

(37) Pei, W. Y.; Li, X. Q.; Bi, R. L.; Zhang, X.; Zhong, M.; Yang, H.; Zhang, Y.; Lv, K. Exosome membrane-modified M2 macrophages targeted nanomedicine: Treatment for allergic asthma. *J. Controlled Release* **2021**, *338*, 253–267.

(38) Li, X. Q.; Zhang, Y. Y.; Pei, W. Y.; Zhang, M. Y.; Yang, H.; Zhong, M.; Kong, X.; Xu, Y.; Zhu, X. L.; Chen, T. B.; Ye, J. J.; Lv, K. LncRNA Dnmt3aos regulates Dnmt3a expression leading to aberrant DNA methylation in macrophage polarization. *FASEB J.* **2020**, *34*, 5077–5091.